Stony Brook University

Studies of Cold Fermionic Systems near the Feshbach Resonance

A Dissertation Presented

by

Lai-Wa Siu

to

The Graduate School

in Partial Fulfillment of the Requirements

for the Degree of

Doctor of Philosophy

in

Physics

Stony Brook University

August 2008

Stony Brook University

The Graduate School

Lai-Wa Siu

We, the dissertation committee for the above candidate for the Doctor of Philosophy degree, hereby recommend acceptance of this dissertation.

Thomas T. S. Kuo – Dissertation Advisor
Professor, Department of Physics and Astronomy

Gerald E. Brown – Chairperson of Defense
Distinguished Professor, Department of Physics and Astronomy

Thomas H. Bergeman
Adjunct Professor, Department of Physics and Astronomy

Roy A. Lacey
Professor, Department of Chemistry

This dissertation is accepted by the Graduate School.

Lawrence Martin
Dean of the Graduate School

Abstract of the Dissertation

Studies of Cold Fermionic Systems near the Feshbach Resonance

by

Lai-Wa Siu

Doctor of Philosophy

in

Physics

Stony Brook University

2008

Cold Fermi gas with a tunable interaction is experimentally realized in trapped cold alkali atoms. Through evaporative cooling these atoms can be brought well into the degenerate regime. In addition, with magnetic field induced Feshbach resonances the underlying interaction between atoms prepared in two different spin states can be manipulated via the Zeeman effect. Cold Fermi atoms can be made to undergo a BCS-BEC crossover, where the ground state wavefunction evolves smoothly from the BCS-type to the BEC-type. The different interaction regimes in the crossover can be characterized by the dimensionless parameter $1/a_s k_F$ de-

fined from the s-wave scattering a_s and the Fermi momentum k_F. At Feshbach resonance, where the scattering length essentially diverges up to $\pm\infty$, $1/a_s k_F = 0$ resulting in a special scenario for a low-density Fermi gas termed the 'unitary limit' by many authors. At such limit cold Fermi gas should exhibit universal behavior in the sense that physical properties becomes independent of the two-body interaction and determined only by k_F. In particular, the total energy at zero-temperature E_0 is expected to depend on k_F through the simple relation $E_0 = \xi E_0^{free}$ where E_0^{free} is the corresponding quantity in a non-interacting gas. The proportionality constant ξ should be an universal constant being the same for any type of underlying particles. In this dissertation we present several studies on cold Fermi gas at and near the unitary limit. Our primary focus is the calculation of ξ with neutron matter. As is well-known, the $^1S_0$ channel of neutron matter has a fairly large scattering length ($a_s = -18.97$fm), therefore ordinary neutron matter is already close to the unitary limit. To obtain ξ accurately we need 'modified' neutron matter much closer to the unitary limit than the ordinary one. By slightly tuning the meson-exchange CD-Bonn potential, neutron-neutron potentials with various $^1S_0$ scattering lengths such as $a_s = -12070$fm and $+21$fm are constructed. Such potentials are renormalized with rigorous procedures to give the corresponding a_s-equivalent low-momentum potentials V_{low-k} , with which the low-momentum particle-particle hole-hole ring diagrams are summed up to all orders, giving the

ground state energy E_0 of neutron matter for various scattering lengths. At the limit of $a_s \to \pm\infty$, our calculated ratio of E_0 to that of the non-interacting case is found remarkably close to a constant of 0.44 over a wide range of Fermi momenta. This result reveals an universality that is well consistent with the recent experimental and Monte-Carlo computational study on low-density cold Fermi gas at the unitary limit. Apart from ground state properties, low-lying excitations also offer lots of insights into the rich physics underlying the BCS-BEC crossover process. We have calculated the quadrupole excitations of cold Fermi gas near the unitary limit using a simple model where atoms are confined in a harmonic oscillator potential. By summing up exactly the ladder diagrams between a pair of interacting atoms to all orders, we first obtained a renormalized atomic interaction which has well defined and identical limits as the scattering length tends to $\pm\infty$. Employing both the Tamm-Dancoff and random phase approximations we obtained the excitation frequency and decay width. The experimentally observed abrupt rise in frequency and an associated large decay width in the radial compression mode and radial quadrupole mode are satisfactorily reproduced by our calculation.

To Koon-Kiu and my parents

Contents

List of Figures

List of Tables

Acknowledgements

The completion of this thesis is made possible under the guidance and encouragement of many people. To star with, I thank Professor Tom Kuo, my thesis advisor, for his supervision during the past four years. He is famous for his big, warm and welcoming smiles. I thank Tom for his patient and step-by-step supervision. Even though cold Fermi gas at the unitary limit is a hard research subject, after a great deal of work we finally got useful result. Without his patience and encouragement, success is not possible. Therefore, my many sincere thanks go to him. I also thank all professors in the Nuclear Theory Group of Stony Brook. I believe all graduate students in the group have enjoyed and impressed by their exciting discussions on various subjects during the regular lunch seminars. Especially, I thank Professor Gerry Brown. I was in his class on nuclear physics, his sharp insights into physics problems impressed and inspired me a lot. I also thank him for his encouragement and useful advice on my thesis work. I thank Dr. Boris Gelman. At the early stage of my thesis work, Boris introduced the subject to me. We have many useful discussion and in particular, he gave me many useful reference papers.

I thank Dima Volja. Dima used to be my office-mate, we spent a lot time chatting and sharing. Thank you so much for your friendship and support.

My special thank goes to Pat Peiliker, the assistant graduate program director, and Professor Laslo Milhaly, the graduate program director. Thanks for your understanding every time I messed up the paper work.

I am so indebted to Koon-Kiu my husband. My gratitude to him is beyond words.

The completion of the work in this thesis is also a journey of Faith. I praise the Lord for I see His hands leading me through every challenge in work, in family, and after all, in the life as a Christian female physicist. Hallelujah!

Chapter 1

Introduction

1.1 Cold atoms and the Feshbach Resonance

The experimental success in trapping and manipulating cold atoms have opened a new era to the study of cold degenerate gas. In a typical setting, 10^{10} neutral alkali atoms are confined by magnetic and/or optical traps to a small region of $\sim 50\mu$m in space, with a central particle density $\sim (10^{13} - 10^{15})\text{cm}^{-3}$. Through evaporative cooling the temperature can be brought down to 10^{-5}K so that quantum degeneracy can be reached. Note that these cold atoms are even more dilute than air molecules at room temperature and atmospheric pressure, which has a density of 10^{22}cm^{-3}. Excellent description on the experimental details including trapping and cooling procedures can be found in Ref.[1].

With cold atoms physicists can experimentally demonstrate the so-called macroscopic quantum phenomena. One classic example is Bose-Einstein condensation (BEC)[2], a situation where a macroscopic number of particles oc-

cupy a single quantum state. Theoretically predicted back in 1924 by Einstein, BEC was first experimentally realized with ^{87}Rb atoms in 1995[3]. From then on experiments on cold atoms has revealed a wide range of exciting phenomena. These experimental success greatly stimulated the growth in theoretical studies of cold quantum systems.

In principle, BEC occurs in cold *bosonic* gas only. Nonetheless, the condensation of 'paired' fermions may be possible under certain circumstances. In fact, the similarity between the Bardeen-Cooper-Schrieffer(BCS) state in fermionic systems and the Bose-Einstein condensed state in bosonic systems have long been pointed out by theoretical physicists[4]. Of special interest is the possibility of creating a BEC of composite molecules by simply increasing the inter-particle attraction of a fermionic gas at low temperature: In the weakly attracting regime, Cooper pairs form via a many-body effect; in the strongly attracting regime where a two-body bound state exists, molecules form and undergo the usual BEC; in between the ground state wavefunction of the whole system should evolve smoothly from the BCS-type to the BEC-type. In many-body theory it is known as the BCS-BEC crossover[4, 5]. Recently, the experimental control on the underlying interaction among cold alkali atoms was made possible through magnetic field induced Feshbach resonances[6–8]. With fermionic ^{6}Li and ^{40}K atoms, many measurements have been done demonstrating various signatures of such crossover, including the observation of (i) a pairing gap[9, 10], (ii) condensation of fermionic pairs[11, 12], and (iii) vortices and vortex arrays[13] on different interaction regimes throughout the crossover.

The successful implementation of magnetic field induced Feshbach reso-

nance is considered an important breakthrough in cold alkali gas experiments. It provides a way to experimentally control the scattering length and alter the effective interaction between cold atoms. Under an external magnetic field, the energy levels of cold atoms are made tunable through the Zeeman effect. Feshbach resonance is the point where the formation of a two-body bound state is energetically possible. As such bound state emerges the scattering length also becomes infinitely long, resulting in a scattering resonance. As an example, the tunability of the scattering length of ^{6}Li around a Feshbach resonance at 834G is shown in Fig.1.1[14]. Tuning the external magnetic field across a Feshbach resonance is equivalent to a continuous increase in the attraction between the atoms until a two-body bound state exists. Beyond such point, the composite molecules which are now bosons can form a Bose-Einstein condensate at sufficiently low temperature.

To probe the ground state properties of cold fermionic atoms around a Feshbach resonance more quantitatively, let us start with the particle density. From the central particle density n_0 in a typical cold alkali gas experiment one can compute the dimensionless diluteness parameter n_0R^3 contrasting the inter-particle distance with the range of the underlying van der Waals potential R. Typically $R \sim 30a_0$(a_0 is the Bohr radius), giving $n_0R^3 \sim 10^{-5} - 10^{-3} \ll 1$. Owing to such 'diluteness', the ground state properties of the gas cloud is essentially characterized just by the two length scales, (i) the s-wave scattering length a_s and (ii) the Fermi momentum at the trap center k_F. It is helpful to introduce a dimensionless strength parameter $1/a_sk_F$ for the characterization of the ground state. For example, when $1/a_sk_F \gg 1$ the scattering length is small and positive signifying the existence of tightly bound molecules, the

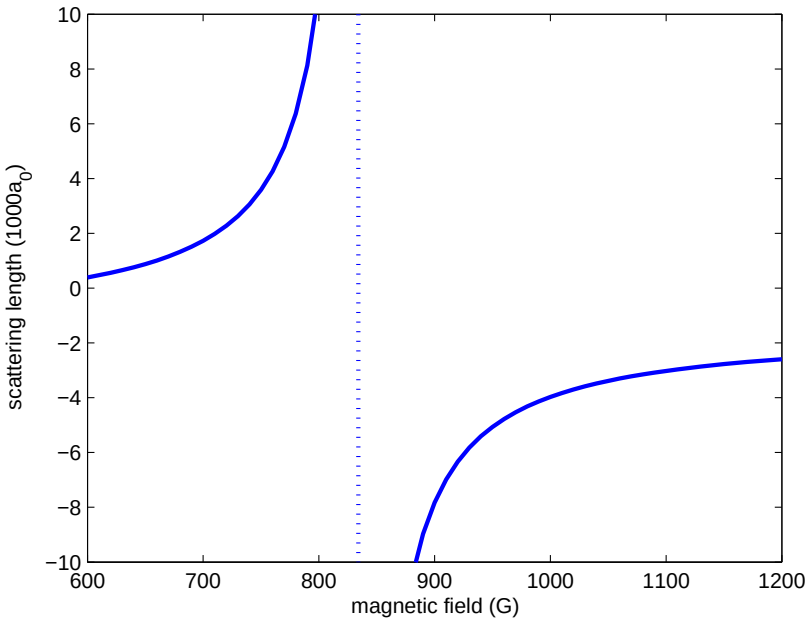

Figure 1.1: The tunability of the s-wave scattering length in a spin mixture of ^{6}Li atoms in the two lowest spin states as described by a fit formula in Ref.[14] which approximates the scattering length in a range between 600G and 1200G to better than 99%. The vertical line indicates the exact position of the resonance field(834G).

system is well into the molecular BEC regime. When $1/a_s k_F \ll -1$ the scattering length is small and negative, the system is in the usual BCS regime.

It is clear from Fig. 1.1 that at a Feshbach resonance the scattering length can be tuned basically up to $\pm\infty$. In other words, the special scenario of $1/a_s k_F = 0$, often referred to as the 'unitary limit', can be achieved. Cold Fermi systems at the unitary limit exhibit very interesting features. A brief review on that is followed in the next section.

Table 1.1: The order of magnitude of various fundamental length scales in a typical cold ^{6}Li experiment. R denotes the range of the van der Waals potential; k_F denotes the Fermi momentum at the trap center; a_s denotes the s-wave scattering length; n_0 denotes the central particle density. The magnitude of a_s under an external magnetic field of 700G, close to a Feshbach resonance at 834G is given. Note that lengths are given in the unit of the Bohr radius $a_0 = 0.529$nm.

R	$30a_0$
k_F^{-1}	$4000a_0$
a_s(at B =700G)	$1000a_0$
n_0R^3	10^{-6}

1.2 The universality at the unitary limit

The term 'unitary limit' originally refers to the situation in a two-body scattering process where the cross section attains its possible maximum. Mathematically that means the particles possess an infinitely long scattering length. In fact, many authors also use such term to describe a low density(small k_F) many-body system with a huge scattering length a_s. Under such conditions the fermions are 'strongly interacting' and a full theoretical description of the system is a challenging task in many-body theory.

Quantitatively, the low-density condition means $n_0R^3 \ll 1$. When the scattering length approaches infinity, the dimensionless parameter $1/a_sk_F$ reaches zero. Satisfying both criteria should result in a special situation where both R and a_s drop out of the many-body problem, leaving k_F as the only relevant length scale, or equivalently k_F^2/m as the only energy scale. Obviously this implies an 'universality' meaning that the properties of the fermionic system depend only on k_F and are independent on the underlying two-body

potential[15–17]. Of much interest and significance is the 'universal' equation of state shared by all cold Fermi gas at zero temperature. The ground state energy E_0 of a two-species fermionic system at the unitary limit can be shown to be simply proportional to that of the non-interacting gas, namely $E_0 = \xi E_0^{free}$ [15] with the proportionality constant ξ being the same for any type of underlying particles. Similar universal behavior is expected to show up also in collective excitations [18–22, 24, 26, 28, 32], and thermodynamic properties [29–33].

The ground state properties of a fermionic system possessing a huge scattering length has aroused interest among theoretical physicists for some time. Back in 1999, Bertsch[34] already formulated a challenge to many-body theorists to clarify the structure of the ground state of a *fictitious* neutron matter interacting with an infinite scattering length. The recent implementation of Feshbach resonance in cold alkali atoms has made the experimental study of fermion gas at and close to the unitary limit possible. The universality at the unitary limit allows such studies to start with very simple model two-body potentials such as a contact interaction.

In this dissertation, we present several studies on cold Fermi gas at and close to the unitary limit. Our major study is based on neutron matter, while the rest are based on simple model systems. The nucleon-nucleon interaction is a realistic two-body potential far more complicated than that in atoms. It is important to demonstrate that neutron matter at the unitary limit indeed have the expected universal equation of state $E_0 = \xi E_0^{free}$ mentioned before, and the numerical value of ξ should be consistent with numerical studies on model cold fermionic systems. In our work traditional many-body approaches

from nuclear physics are employed, including the use of Brueckner G-matrix and the recently developed low-momentum nucleon-nucleon interaction V_{low-k}. More details are given in the next two sections.

1.3 Neutron matter at the unitary limit

The primary focus in this dissertation is the calculation of the ground state energy E_0 of cold fermi gas at the unitary limit which should have the form $E_0 = \xi E_0^{free}$ with the constant ξ being the same for all underlying particles. The four most recent experimental value of ξ from cold alkali gas fall between 0.36-0.46[32, 35–37], with relatively large error bars($\sim 10\%$). By far the best estimate on ξ is from quantum Monte Carlo methods. Astra *et. al.* obtained 0.42(1) based on a square well potential with a particle density $nR_0^3 = 10^{-6}$ (where R_0 is the potential range)[39]. Carlson *et. al.* obtained 0.44(1) based on a 'cosh potential', with a particle density $n\mu^{-3} = 0.020$ (where $2/\mu$ is the effective range)[38].

In our work the determination of ξ is based on neutron matter. Ordinary low-density neutron matter is already quite close to the unitary limit owing to its large s-wave scattering length $a_s \sim 19$fm in the $^1S_0$ channel. To study neutron matter at the unitary limit, we shall slightly modify the usual neutron-neutron interaction through a manual tuning on the mass of σ meson in the high-precision meson-exchange CD-Bonn nucleon-nucleon(NN) potential[40]. Exchanging a lighter meson should generate a stronger attraction, making the scattering length a_s more negative. In this way we generate 'tuned' NN interaction associated with various values of $^1S_0$ scattering lengths

ranging from -10fm to -12000fm. To obtain the ground state energy we shall sum up the low-momentum particle-particle hole-hole (*pphh*) ring diagrams to all orders based on a model space method. The inclusion of hole-hole correlation in such ring diagram summation is expected to give improved result over the traditionally used Brueckner-Hartree-Fock method on the equation of state. The tuned nucleon potentials are first renormalized by integrating out the high-momentum components beyond a certain decimation scale Λ. An infinite order summation of *pphh* ring diagrams within the finite model space $k \leq \Lambda$ is then followed giving finally the ground state energy of neutron matter. For the renormalization we have employed two approaches, one results in the Brueckner G-matrix[45, 46] and the other V_{low-k} which is a recently developed low-momentum interaction[50–55]. In Chapter 3 we shall show that these two approaches give almost identical computation result, nonetheless, the V_{low-k} approach offers a much more direct and simpler calculation. A brief introduction of both is given in the next section.

We have obtained the equation of state for low-density neutron matter with Fermi momentum k_F ranging from $0.8 - 1.5\text{fm}^{-1}$, or in terms of the particle density $n = (1.73 - 11.40) \times 10^{-2}\text{fm}^{-3}$. At the limit $a_s \to \pm\infty$, resulted values on $\xi = E_0/E_0^{free}$ all lies within a narrow window of 0.437-0.448[41]. This clearly confirms a universality over $n\Lambda^{-3} = (1.4 - 9.4) \times 10^{-3} \ll 1$. The numerical value of ξ is not just consistent with experimental values from cold atoms, but also in excellent agreement with the numerical result from quantum Monte Carlo calculations. Let us stress again that neutron-neutron interaction differs greatly from the van der Waals potential in cold atoms, or the model potentials of square well and cosh function used in Monte Carlo calculations.

Table 1.2: Important length scales in our calculation of the ground state energy of neutron matter at the unitary limit. Λ is the decimation scale used in the renormalization of the tuned CD-Bonn potential giving a scattering length $a_s = -12000$fm in the $^1S_0$ channel.

Λ	2.3fm^{-1}
k_F	0.8-1.5fm^{-1}
a_s(tuned CD-Bonn)	-12000fm
$n\Lambda^{-3}$	$(1.4 - 9.4) \times 10^{-3}$

The fact that low-density cold Fermi gas all share a unique equation of state provides an excellent illustration of the underlying universality.

In our computation on neutron matter we have 'tuned' the meson-exchange CD-Bonn potential. Such 'tuning' is a manual adjustment on the mass of σ meson and thus on the scattering length in the $^1S_0$ channel. To obtain $a_s = -12000$fm we have decreased the mass of σ by about 2%(10MeV). Worth mentioning is that the decrease on meson masses may come naturally from the density dependence of nucleon potential itself. The Brown-Rho scaling[42, 43] suggests that the in-medium mass(m^*) of ρ, ω and σ should decrease linearly with the nuclear density n according to $m^*/m = 1 - Cn/n_0$, where C is a constant of value $\sim 15\%$ and n_0 is the nuclear saturation density. The full consideration on the such density modification on neutron potential should include the enhancement of attraction from σ and also the repulsion from ρ and ω as well. Whether the combined effect could result in a huge scattering length is out of the scope of this dissertation. The equation of state of nuclear matter with Brown-Rho scaling incorporated is of much interest and is under study[44].

1.4 Renormalization of NN interaction

In microscopic calculations on neutron matter, suitably renormalized nucleon-nucleon(NN) interaction must be employed. Both the repulsive hard core and the tensor-force which is highly singular at short distances make the bare NN potentials unsuitable for direct calculations. Traditionally, the Brueckner G-matrix[45, 46] is used in place of the bare NN potential. It is defined by

$$G_{ijkl}(\omega) = V_{ijkl} + \sum_{rs} V_{ijrs} \frac{Q(rs)}{\omega - k_r^2 - k_s^2 + i0^+} G_{rskl}(\omega) \tag{1.1}$$

where k_r^2 stands for the kinetic energy $\hbar^2 k_r^2/2m$ and similarly for k_s^2. Q is the Pauli projection operator which ensures that the intermediate states must be particle states.

$$\begin{aligned} Q(rs) &= 1, if\ k_s, k_r > k_F \\ &= 0, otherwise. \end{aligned} \tag{1.2}$$

As obvious from Eqn.1.1, the G-matrix approach renormalizes the bare NN potential through a particle-particle ladder resummation. Note also that the Brueckner G-matrix is energy dependent in the sense that it is a function of the 'starting energy' ω, which must be determined self-consistently[45, 46].

Motivated by the renormalization group(RG) and effective field theory(EFT), the low-momentum NN potential, denoted as V_{low-k}[50–55], is a recently developed effective NN interaction. From a EFT perspective, because low-energy physics are insensitive to the details of the high-energy dynamics, there exists many Hamiltonians possessing the same low-momentum structure that give

rise to the same low-energy physics, while differing only in the high-momentum region. Intuitively one can construct a simple effective low-momentum interaction by integrating out all high-momentum components beyond a cut-off Λ, under the condition that the low-energy phase shifts and the deuteron pole remain preserved. Since realistic NN potentials such as CD-Bonn[40], Argonne[47], Nijmegan[48] and Idaho[49] are all constructed to reproduce experimental determined phase shifts up to an energy $E_{lab} \approx 300$MeV, by choosing a $\Lambda \simeq 2\text{fm}^{-1}$ one can obtain an effective NN potential with the model-dependent high-momentum components 'removed'.

More specifically, the renormalization procedure in the construction of V_{low-k} is based on a T-matrix equivalence method [50–55]. One requires V_{low-k} to satisfy

$$T_{low-k}(p', p, p^2) = V_{low-k}(p', p) + \int_0^\Lambda q^2 dq \frac{V_{low-k}(p', q) T_{low-k}(q, p, p^2)}{p^2 - q^2 + i0^+}, \quad (1.3)$$

where T_{low-k} is the low-momentum components of the original T-matrix, namely

$$T(p', p, p^2) = T_{low-k}(p', p, p^2); \ (p', p) \leq \Lambda. \quad (1.4)$$

In other words, the half-on-shell matrix elements of T are preserved up to the cut-off Λ. Notice that the intermediate states in Eqn. 1.3 is from zero to Λ. This should be contrasted to the definition of the original T-matrix which is

$$T(k', k, k^2) = V(k', k) + \int_0^\infty q^2 dq \frac{V(k', q) T(q, k, k^2)}{k^2 - q^2 + i0^+}. \quad (1.5)$$

It can be shown that the construction of V_{low-k} is a renormalization group

decimation[56]. Recent works demonstrates that the V_{low-k}'s derived from various bare NN potentials such as CD-Bonn, Argonne, Nijmegan and Idaho all flow to a unique potential as the decimation scale is brought down to around 2fm^{-1}[50–55]. The resulted 'unique' V_{low-k} is smooth and energy-independent. In contrast, the energy-dependence in Brueckner G-matrix often complicates the numerical calculations. An in-depth review on V_{low-k} can be found, for example, in Ref.[54].

1.5 Dissertation Outline

In this dissertation, we focus on cold Fermi gas at and near the unitary limit where Fermi atoms are strongly interacting. Since the experimental investigation is mainly on cold alkali atoms at broad Feshbach resonances, therefore in Chapter 2 we shall first discuss the underlying mechanism of such coupled-channel scattering resonance. To illustrate its main features a simple and exactly solvable model shall be employed.

In Chapter 3, we present our major study, namely the calculation on the ground state energy of neutron matter at and close to the unitary limit. First, we shall explain how we produce neutron-neutron interactions with various scattering lengths by slightly tuning the high precision CD-Bonn potential. These tuned neutron potentials must be renormalized for microscopic calculation. The renormalization procedures will be discussed. In particular we shall emphasize the advantage of using the recently developed low-momentum nucleon-nucleon interaction V_{low-k}. A model-space approach is used to sum up the low-momentum particle-particle hole-hole ring diagrams to all orders,

giving the equation of state. Such model space ring computation will be presented with details. Our result on the equation of state is not just consistent with the most recent cold alkali gas experimental findings, but in excellent agreement with quantum Monte Carlo computations.

We further study the quadrupole excitations of cold Fermi gas at the unitary limit. Assuming atoms are confined in a harmonic oscillator and interact via a separable potential of the Yukawa form, we calculate the quadrupole excitations with the random phase approximation. We obtained a similar abrupt rise in the excitation spectrum and the associated large decay width as observed in experiments. This work can be found in Chapter 4.

We have also applied the widely used Brueckner-Hartree-Fock(BHF) method to cold Fermi gas at the unitary limit. With a model potential we derived analytically the form of the Brueckner G-matrix for low-density Fermi gas. From a fully self-consistent BHF computation we obtain an equation of state at the unitary limit. The result, presented in Chapter 5, is in excellent agreement with quantum Monte Carlo calculation on the normal ground state of cold Fermi gas.

A summary of this dissertation is contained in Chapter 6.

Chapter 2

Separable Coupled-Channel Model and Magnetic Field Induced Feshbach Resonance

2.1 Feshbach resonance in cold alkali gas

Feshbach resonance [57] originally refers to a resonance in neutron scattering due to the formation of a quasi-bound state between the scatterer and the incident particle. Recently, magnetic field induced Feshbach resonance is realized in trapped cold alkali gas[6–8]. By tuning an external magnetic field, the energy of a quasi-bound state in a closed scattering channel is Zeeman shifted and made very close to the energy threshold of an open channel, giving rise to a magnetic-field induced scattering resonance. This resonance has many interesting features and has opened a new era to the study of cold quantum gas. It serves as an experimental control mechanism to tune the scattering

length of alkali atoms over a wide range, essentially from positive to negative infinity. Through such process, the inter-atomic effective interaction could also be experimentally controlled. As a result, cold alkali gases has provided us a unique many-body system with a tunable interaction.

The ground state electronic structure of alkali atoms is very simple to describe. It consists of closed shells and an extra electron occupying a s-orbit in a higher shell. The nuclear spin is coupled to the electron spin via the hyperfine interaction. In cold alkali gas experiments temperature of the gas cloud is so low that the hyperfine states are the only relevant degrees of freedom. During a close encounter with an incoming particle, an alkali atom can be scattered from one hyperfine state to another. In other words, the scattering process of cold atoms is a coupled-channel problem. Typically, cold alkali gas atoms are first prepared in an equal mixture of two hyperfine states. An external magnetic field is then used to induce a s-wave resonance. For example, a s-wave Feshbach resonance can be observed at around 202G with trapped ^{40}K atoms prepared in states $|f = 9/2, m_f = -7/2\rangle$ and $|f = 9/2, m_f = -9/2\rangle$[11].

With a coupled-channel theory, the Feshbach resonance demonstrated in cold alkali gas can be studied through a rigorous formulation from the underlying microscopic physics. A thorough discussion can be found, for example, in Ref.[58]. The resonance mechanism can be illustrated starting from a two-channel Hamiltonian of the form

$$H = \begin{pmatrix} -\nabla^2 & 0 \\ 0 & -\nabla^2 + \Delta \end{pmatrix} + \begin{pmatrix} V_{11} & V_{12} \\ V_{21} & V_{22} \end{pmatrix}. \tag{2.1}$$

The two scattering channels, 1 and 2, represent respectively an open and a closed channel in an inter-atomic scattering process. V_{11} and V_{22} denotes the atomic interactions for these channels respectively, while V_{12} denotes the inter-channel coupling.

Feshbach resonances demonstrated in cold alkali atoms involve a shallow bound state in the closed channel. The resonance mechanism is best illustrated with a figure. Fig.2.1 is a schematic illustration of a coupled-channel Feshbach resonance. The energy E_b of a shallow bound state in the closed channel is shifted as Δ is tuned. As E_b gets close to the threshold of the open channel, the system can be easily scattered into the closed channel before decaying back to the open channel, leading to a resonance.

To describe a Feshbach resonance more quantitatively, one need to obtain a relation between the scattering length a_s and the tuning parameter Δ in order to obtain the exact resonance position Δ_{FR}. Also of interest is the width of the resonance Γ. To a good approximation, the behavior of a_s in the proximity of a resonance can be described by the simple expression

$$a = a_{nr}\left(1 + \frac{\Gamma}{\Delta - \Delta_{FR}}\right). \tag{2.2}$$

where a_{nr} represents a non-resonant scattering length. For example, the Feshbach resonance of ^{6}Li at 830G can be described by the following fit formula to better than 90% in a wide range of magnetic field B from 600G to 1200G:

$$a_s(B) = a_{bg}\left(1 + \frac{\Delta B}{B - B_0}\right)(1 + \alpha(B - B_0)) \tag{2.3}$$

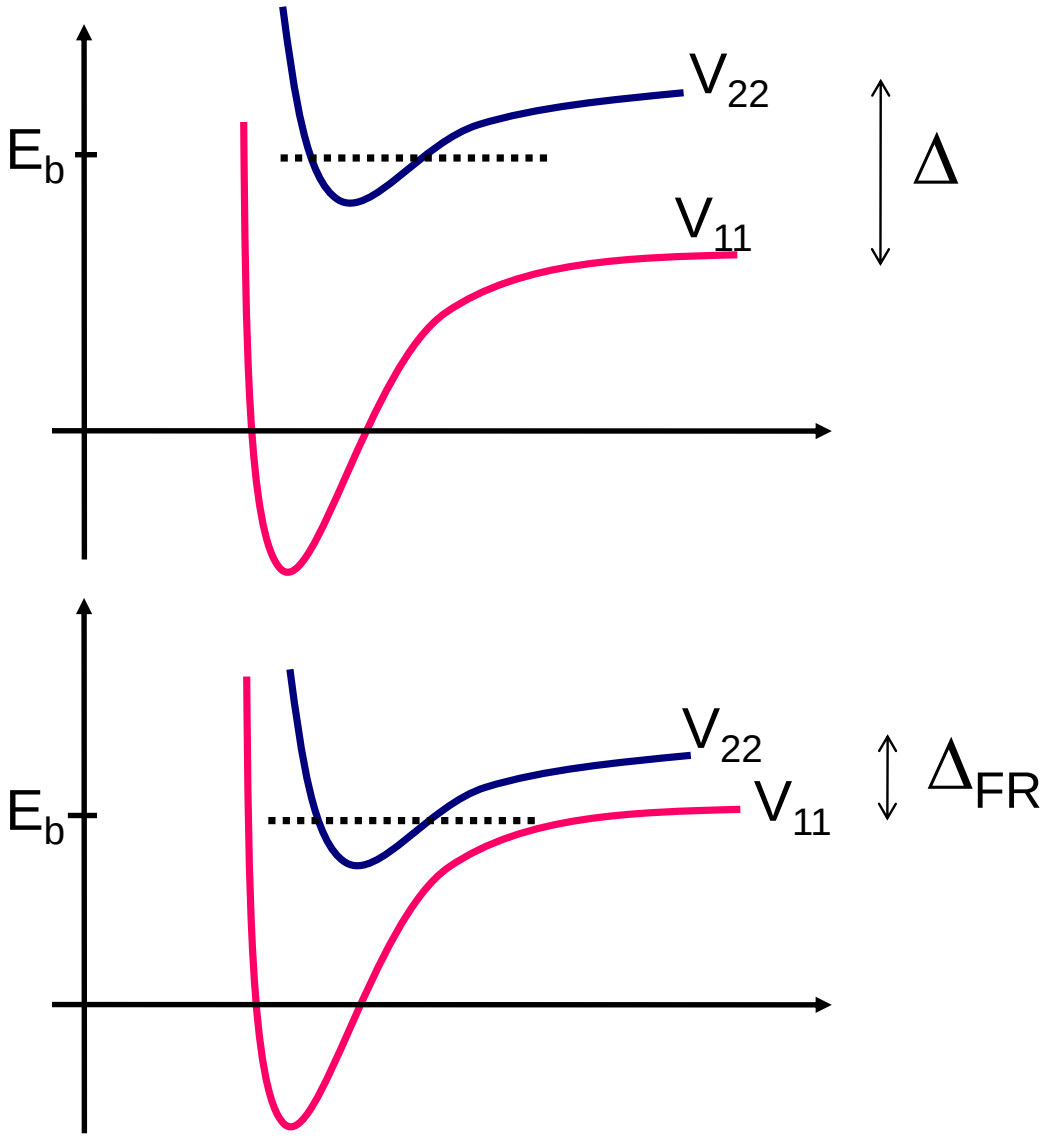

Figure 2.1: Schematic illustration of coupled-channel Feshbach resonance. At resonance, the energy of a bound state in the closed channel is made very close to the threshold of the open channel.

where ΔB, B_0, a_{bg} and α are fitting parameters of values 300G, 834.15G, -1405a_0 and 0.040kG^{-1} (a_0 is the Bohr radius)[14].

Γ is an important physical parameter characterizing the 'broadness' of a Feshbach resonance. In cold alkali gas experiments, various *broad* and *narrow*

Feshbach resonances are predicted and observed. For example, in the experimental study of the two lowest hyperfine states of ^{6}Li, a broad s-wave Feshbach resonance is found at $\sim$ 830G, and a narrow one at $\sim$ 540G[12, 59]. One can show that Γ is related to the effective range r_e of the scattering.

As mentioned in Chapter 1, dilute Fermi gas with both a short range interaction and a large scattering length should exhibit universal behavior in the sense that the only relevant length scale left in the many-body system should be the Fermi momentum k_F. Nonetheless, it have been stressed by many authors that such universality could be expected only at *broad* Feshbach resonances[60, 61], which means the effective range r_e should also be sufficiently small (compared to k_F^{-1}) for universality to hold. Of more interest is that a coupled-channel Feshbach resonance can be effectively mapped to an single-channel one if it is broad [61]. It follows then in a theoretical study of the universal properties of a many-body cold fermionic systems near the unitary limit, it is sufficient to consider the simple scenario where a broad scattering resonance occurs in a single channel.

To address these issues, the next section is devoted to a more in-depth discussion on the coupled-channel nature of the magnetic field induced Feshbach resonance in cold Fermi gas experiments. With the use of an exactly solvable model, we illustrate how one can derive analytically an expression relating the scattering length a_s and the tuning parameter Δ. Based on which the relationship of the width Γ and the effective range r_e can be studied. From our model it is clear that a large Γ implies a small r_e. We shall present a procedure for constructing an effective single-channel potential that would reproduce the same T-matrix for the underlying coupled-channel Hamiltonian. Being con-

sistent with the result in Ref.[61], such procedure is unambiguous only if Γ is large.

2.2 Exactly solvable model in coupled-channel Feshbach Resonance

2.2.1 Coupled-channel separable model of Feshbach resonance

We consider a model two-component system and assume a Hamiltonian of the form in Eqn.2.1. To study the Feshbach resonance for such model, the physical quantity of primary interest would be the reactance matrix R defined by

$$\begin{pmatrix} R_{11} & R_{12} \\ R_{21} & R_{22} \end{pmatrix} = \begin{pmatrix} V_{11} & V_{12} \\ V_{21} & V_{22} \end{pmatrix} + \begin{pmatrix} V_{11} & V_{12} \\ V_{21} & V_{22} \end{pmatrix} \begin{pmatrix} G_1^{\mathcal{P}}(\omega) & 0 \\ 0 & G_2^{\mathcal{P}}(\omega, \Delta) \end{pmatrix} \begin{pmatrix} R_{11} & R_{12} \\ R_{21} & R_{22} \end{pmatrix} \tag{2.4}$$

where the propagators are

$$G_1^{\mathcal{P}}(\omega) = \frac{\mathcal{P}}{\omega - (-\nabla^2)} \qquad G_2^{\mathcal{P}}(\omega, \Delta) = \frac{\mathcal{P}}{\omega - (-\nabla^2) - \Delta}. \tag{2.5}$$

Note that the principal value boundary condition, denoted by $\mathcal{P}$, is imposed. Once an full analytic expression on R is obtained, one can deduce the molecular bound state energies from the poles and derive the T matrix and other scattering parameters in a straight forward way.

To solve for R, it is convenient to consider the momentum space coupled

integral equations. As an example, R_{11} and R_{21} satisfy

$$\begin{aligned} R_{11}(k,k',\omega) &= V_{11}(k,k') + \frac{2}{\pi}\mathcal{P}\int \frac{V_{11}(k,q)R_{11}(q,k',\omega)}{\omega - q^2} q^2 dq \\ &\quad + \frac{2}{\pi}\mathcal{P}\int \frac{V_{12}(k,q)R_{21}(q,k',\omega)}{\omega - q^2 - \Delta} q^2 dq, \end{aligned} \tag{2.6}$$

where the two-particle relative momenta are denoted by k, k' and q. The equations for the other components of R are of similar forms and are omitted.

We assume that the potentials are separable in the form

$$V_{ij}(k,k') = \alpha_{ij} f_i(k) f_j(k');\ i,j = 1,2, \tag{2.7}$$

with $f_i(k)$ being a Yukawa-type function, namely

$$f_i(k) = \frac{1}{\mu_i^2 + k^2};\ i = 1,2. \tag{2.8}$$

α_{ij} and μ_i^{-1} represent respectively the strengths and ranges of the interactions. In coordinate space, the above separable potential corresponds to a non-local potential of the form $e^{-\mu_i r} e^{-\mu_j r'}/(rr')$. It is readily seen that the solutions of the integral equations above will also have a separable form, namely

$$R_{ij}(k,k',\omega) = \lambda_{ij}(\omega) f_i(k) f_j(k');\ i,j = 1,2. \tag{2.9}$$

The functions λ_{ij} are

$$\lambda_{11}(\omega) = \frac{\alpha_{11}(1 - \alpha_{22} I_2(\omega)) + \alpha_{12}\alpha_{21} I_2(\omega)}{(1 - \alpha_{11} I_1(\omega))(1 - \alpha_{22} I_2(\omega)) - \alpha_{12}\alpha_{21} I_1(\omega) I_2(\omega)}, \tag{2.10}$$

$$\lambda_{21}(\omega) = \frac{\alpha_{21}(1-\alpha_{11}I_1(\omega)) + \alpha_{11}\alpha_{21}I_1(\omega)}{(1-\alpha_{11}I_1(\omega))(1-\alpha_{22}I_2(\omega)) - \alpha_{12}\alpha_{21}I_1(\omega)I_2(\omega)}, \tag{2.11}$$

and similarly for λ_{22} and λ_{12}. I_1 and I_2 are integrals

$$I_1(\omega) = \frac{2}{\pi}\,\mathcal{P}\int_0^\infty \frac{f_1(k)^2}{\omega - k^2}k^2\mathrm{d}k \tag{2.12}$$

$$I_2(\omega) = \frac{2}{\pi}\,\mathcal{P}\int_0^\infty \frac{f_2(k)^2}{(\omega-\Delta) - k^2}k^2\mathrm{d}k. \tag{2.13}$$

Note that I_2 is dependent on the Zeeman shift Δ. Substituting $f_i(k)$ as given by Eqn.2.8, we obtain the explicit form of I_i as

$$\begin{aligned} I_i(\omega) &= \frac{\Omega - \mu_i^2}{2\mu_i(\Omega+\mu_,^2)^2},\ \Omega \geq 0, \\ &= -\frac{1}{2\mu_i(\sqrt{(-\Omega)}+\mu_i)^2},\ \Omega < 0. \end{aligned} \tag{2.14}$$

In the above Ω stands for ω for $i = 1$, and $(\omega - \Delta)$ for i=2.

2.2.2 Model studies of Feshbach resonance

To study Feshbach resonance, it is important to first explore the behavior of the molecular bound states. The bound state energies, E, as determined by the poles of R, must satisfy

$$(1-\alpha_{11}I_1(E))(1-\alpha_{22}I_2(E)) - \alpha_{12}\alpha_{21}I_1(E)I_2(E) = 0. \tag{2.15}$$

Observe that by setting $\alpha_{12} = \alpha_{21} = 0$, we can recover the uncoupled case and E should be given by the energies of the individual bound states in each

channel, which were found to be

$$\sqrt{-E} = \sqrt{\frac{-\alpha_{11}}{2\mu_1}} - \mu_1 \text{ (channel 1)} \tag{2.16}$$

$$\sqrt{-(E-\Delta)} = \sqrt{\frac{-\alpha_{22}}{2\mu_2}} - \mu_2 \text{ (channel 2).} \tag{2.17}$$

Thus each individual channel contains at most one bound state as the attractive potential gets stronger. This simple spectrum greatly simplifies the study of the coupled case. For a weak coupling scenario, which is true in experiments, the position of resonance can be crudely determined by requiring the energy of the bound state in the closed channel to be zero. An exact analytic result on the position of the resonance was found to be

$$\Delta_{FR} = \left(\sqrt{\frac{\alpha_{12}\alpha_{21}}{4(\frac{\alpha_{11}}{2\mu_1} + \mu_1^2)\mu_1\mu_2}} - \frac{\alpha_{22}}{2\mu_2} - \mu_2 \right)^2 . \tag{2.18}$$

As Δ is swept across Δ_{FR}, the occurrence of the resonance should reflect in the scattering parameters. The scattering parameters in the open channel can be analytically obtained by the effective-range approximation on the phase shift δ_{11}:

$$k_0 \cot \delta_{11} = -\frac{1}{R_{11}(k_0, k_0, k_0^2)} \equiv -\frac{1}{a_s} + \frac{1}{2} r_e k_0^2 + O(k_0^4) \tag{2.19}$$

where $k_0^2 \equiv \omega$ denotes the incident energy, a_s and r_e denote the scattering length and effective range respectively. For simplicity, here we write down the

results for the case $\mu_1 = \mu_2 = \mu$:

$$a_s = \frac{C}{A} \tag{2.20}$$

$$r_e = \frac{2}{C}\left(\frac{AD}{C} - B\right) \tag{2.21}$$

where

$$A = \mu^2(\mu^2 + \frac{\alpha_{11}}{2\mu})(\frac{\alpha_{22}}{2\mu} + (\mu + \sqrt{\Delta})^2) - \frac{\alpha_{12}\alpha_{21}}{4} \tag{2.22}$$

$$B = (2\mu^2 - \frac{\alpha_{11}}{2\mu})(\frac{\alpha_{22}}{2\mu} + (\mu + \sqrt{\Delta})^2) + \frac{\alpha_{12}\alpha_{21}}{4\mu^2} - \mu^2(\mu^2 + \frac{\alpha_{11}}{2\mu})(1 + \frac{\mu}{\sqrt{\Delta}}) \tag{2.23}$$

$$C = \frac{\alpha_{11}\alpha_{22}}{2\mu} - \frac{\alpha_{12}\alpha_{21}}{2\mu} + \alpha_{11}(\mu + \sqrt{\Delta})^2 \tag{2.24}$$

$$D = -\alpha_{11}(1 + \frac{\mu}{\sqrt{\Delta}}). \tag{2.25}$$

It is obvious that $\Delta = \Delta_{FR}$ is equivalent to the condition of $A = 0$. As resonance is approached, $\Delta \to \Delta_{FR}$ and $A \to 0$ resulting in

$$a_s \to \pm\infty \qquad r_e \to -\frac{2B}{C}. \tag{2.26}$$

Fig.2.2 shows the behavior of a_s and r_e for a broad and a narrow Feshbach resonance from the exact expressions in Eqn.2.20 and Eqn.2.21. As shown from the plots, the width of a resonance in a_s has a definite relationship with the magnitude of r_e at resonance. A broader resonance associates with a smaller residue effective range. In cold alkali gas experiments, scattering length was measured as a function of an external magnetic field and both broad and narrow resonances were observed. As mentioned before, ^{6}Li gas exhibits a

broad resonance at $\sim$ 830G and a narrow resonance at $\sim$ 540G[12, 59]. In our model, the relationship between the width of a resonance and the effective range can be studied analytically.

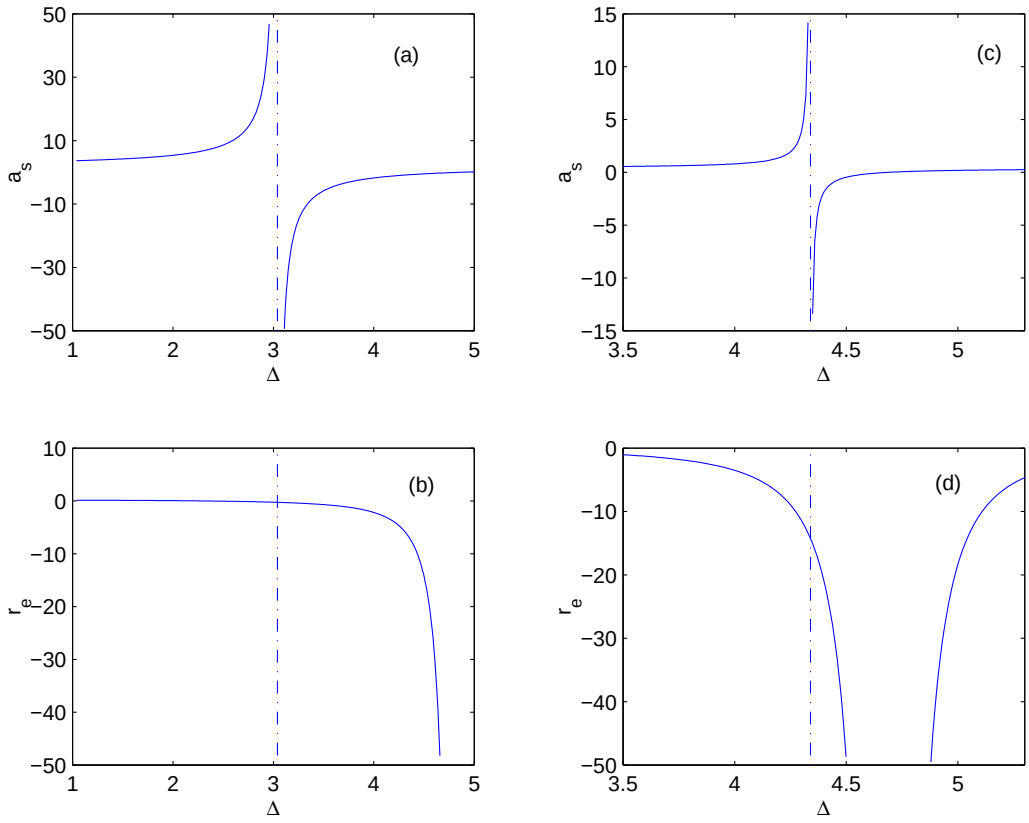

Figure 2.2: Scattering length a_s and effective range r_e of a broad and a narrow Feshbach resonance where $\mu_1 = \mu_2 = \mu$. The exact position of the resonance is marked by the dash-dotted line. (a) and (b) belong to a broad resonance, with $\mu = 10.0$, $\alpha_{11} = -1.1$ $(2\mu^3)$, $\alpha_{11} = \alpha_{21} = 0.1$ α_{11}, $\alpha_{22} = -1.5$ $(2\mu^3)$. (c) and (d) belong to a narrow resonance with $\mu = 10.0$, $\alpha_{11} = -2.0$ $(2\mu^3)$, $\alpha_{11} = \alpha_{21} = 0.1$ α_{11}, $\alpha_{22} = -1.5$ $(2\mu^3)$.

As from Eqn.2.20, the geometric curve relating a_s and the variable $(\mu + \sqrt{\Delta})^2$ is an exact hyperbola with the asymptotes giving the position of the resonance. It is natural to define the width of a resonance Γ as the semi-major

axis which was found to be

$$\Gamma = \frac{\alpha_{12}\alpha_{21}}{\mu(\mu^2 + \frac{\alpha_{11}}{2\mu})^2}. \tag{2.27}$$

Observe that $-\alpha_{11}/(2\mu) = \mu^2$ is the threshold for Channel 1 to contain a bound state. Thus the width of a Feshbach resonance in our model, apart from the trivial dependence on α_{12},α_{21} and μ , is controlled by the position of the bound state in the open channel. A shallow bound state could help producing a broader resonance. As shown above, as a resonance is approached, r_e will approach a limit $-\frac{2B}{C}$ which can be expressed explicitly in terms of Γ as

$$r_e \to -\frac{2B}{C} = \frac{3}{\mu} - \frac{4}{\Gamma}(1 + \frac{\mu}{\sqrt{\Delta_{FR}}}). \tag{2.28}$$

Thus a broad resonance is associated with a slightly negative r_e as in Fig.2.2. The behavior of r_e is very crucial in the study of scattering resonance because it reflects the energy dependence of the phase shift and directly relates to the behavior of the system around the unitary limit.

2.2.3 Complex T-matrix and the unitary limit

In a single channel scattering process, the on shell matrix element of T matrix, $T(k_0, k_0, k_0^2)$, is related to the phase shift δ by

$$k_0 T(k_0, k_0, k_0^2) = -\sin\delta\, e^{i\delta} \tag{2.29}$$

In two-body scattering theory, 'unitary limit' refers to the point where $\delta = \pi/2$. When such limit is reached, $T(k_0, k_0, k_0^2)$ becomes purely imaginary and the scattering cross section attains its maximum. In our coupled-channel model, we define the unitary limit in the open channel as the point where

$$\delta_{11} = \frac{\pi}{2} \quad \text{and} \quad T_{11}(k_0, k_0, k_0^2) = -\frac{i}{k_0}. \tag{2.30}$$

We shall derive a full analytic expression on T_{11} and to study its energy dependence around Feshbach resonance and the unitary limit. To proceed, note that T matrix can be obtained from R matrix by

$$T = R + R \begin{pmatrix} -i\pi\delta(\omega - (-\nabla^2)) & 0 \\ 0 & -i\pi\delta(\omega - (-\nabla^2) - \Delta) \end{pmatrix} T \tag{2.31}$$

where T and R are the 2×2 matrices:

$$T = \begin{pmatrix} T_{11} & T_{12} \\ T_{21} & T_{22} \end{pmatrix}, \tag{2.32}$$

$$R = \begin{pmatrix} R_{11} & R_{12} \\ R_{21} & R_{22} \end{pmatrix}. \tag{2.33}$$

With R being separable, T also admits a solution of a separable form and we define

$$T_{ij}(k, k', \omega) = \eta_{ij}(\omega) f_i(k) f_j(k'); \ i, j = 1, 2. \tag{2.34}$$

The open channel component of T, T_{11}, is easy to solve in the low-energy regime where $\omega \equiv k_0^2 < \Delta$ is assumed. With such assumption T_{11} is solely

determined by R_{11}. By substituting the solution of R we have

$$\eta_{11}(k_0^2) = \frac{\lambda_{11}(k_0^2)}{1 + ik_0\lambda_{11}(k_0^2)f_1(k_0)f_2(k_0)}. \tag{2.35}$$

The real and imaginary parts of the on-shell matrix element $T_{11}(k_0, k_0, k_0^2)$ around both a broad and a narrow Feshbach resonance are plotted in Fig.2.3, each for several values of the incident energy. The unitary limit is the location of the sharp peak in the plot of the imaginary part. The exact positions of the resonances are marked as well. For a broad resonance, Feshbach resonance and the unitary limit occurs at the same point where $\Delta = \Delta_{FR}$. For a narrow resonance, the position of the unitary limit exhibits a stronger energy dependence and does not necessarily coincide with the position of the resonance. In fact, this can be understood analytically by performing an expansion in k_0 on $T_{11}(k_0, k_0, k_0^2)$. It can be trivially shown that when resonance occurs, i.e. $1/a_s = 0$,

$$T_{11}(k_0, k_0, k_0^2) = -\frac{i}{k_0} - \frac{r_e}{2} + i\frac{r_e^2}{4}k_0 + O(k_0^2) \tag{2.36}$$

where r_e is the effective range in the open channel. Notice that r_e enters naturally into the energy expansion above because $T_{11}(k_0, k_0, k_0^2)$ is determined by $R_{11}(k_0, k_0, k_0^2)$ as from Eqn.2.35. As concluded in the previous section, a broad resonance has a small residue r_e. Thus in the above expansion, for low energies the real part vanishes and unitary limit is also reached at resonance.

2.2.4 Effective single-channel potential

In the theoretical study on BCS-BEC crossover, a single channel model is often used, with a simple effective inter-atomic interaction like a contact interaction. However, in trapped alkali gas experiments, the Feshbach resonance is coupled-channel in nature. Whether a coupled-channel Feshbach resonance can be reduced to an effective single-channel resonance aroused some discussions[60, 61]. It has been pointed out that an effective single-channel formalism is possible only if the original coupled-channel resonance is *broad*. Here, we shall illustrate this with our separable model.

First, observe that our single-channel separable model exhibits one and only one Feshbach resonance which is always broad. To see this, we consider the simple case of a single-channel separable potential of the form $V(k,k') = \alpha f(k)f(k')$, where $f(k) = 1/(\mu^2 + k^2)$. Following the derivation in Section 2.2.2, the scattering length and effective range were found to be

$$a_s = \frac{\alpha}{\mu^2(\mu^2 + \frac{\alpha}{2\mu})} \tag{2.37}$$

$$r_e = \frac{1}{\mu} - \frac{4\mu^2}{\alpha}. \tag{2.38}$$

Therefore, there is one and only one broad resonance at $\alpha = -2\mu^3$. At that point, the residue value of r_e is $3/\mu$. This implies that for a short range interaction, r_e is almost zero at resonance.

Since all broad resonances should exhibit universal behavior, a broad resonance in the coupled-channel case should be able to reduce to an effective single-channel one. To see this, we consider the simple case where $\mu_1 = \mu_2$.

We define an effective strength

$$\tilde{\alpha}(\omega) = \alpha_{11} + \alpha_{12}\alpha_{21}\frac{I_2(\omega)}{1 - \alpha_{22}I_2(\omega)}. \tag{2.39}$$

By direct substitution, it is easy to verify that a single-channel separable potential with a strength $\tilde{\alpha}(\omega)$ would reproduce the same R matrix as the open channel component R_{11} of a coupled-channel potential with potential strengths α_{11}, α_{12}, α_{21} and α_{22}. We shall study the energy dependence $\tilde{\alpha}(\omega)$ around a Feshbach resonance. Since $I_2(\omega)$ is known an energy expansion can be done exactly. The position of the coupled-channel potential is given by $\Delta = \Delta_{FR}$. Using such condition, we have at resonance

$$\tilde{\alpha}(\omega) = -2\mu^3 - 8\mu^2(1 + \frac{\mu}{\sqrt{\Delta_{FR}}})\frac{1}{\Gamma}\,\omega + O(\omega^2). \tag{2.40}$$

where Γ is the width of the coupled-channel resonance defined in Eqn.2.27. In the low energy regime, $\tilde{\alpha}(\omega)$ can be considered energy-independent for a resonance with a large Γ. In this way we have demonstrated a procedure to construct an effective single-channel potential for a broad coupled-channel Feshbach resonance.

2.3 Conclusion

We have reviewed the mechanism of Feshbach resonance in cold alkali gas experiments and presented a coupled-channel model for such resonance with separable potentials of Yukawa form. We deduced the condition for resonance and presented exacted analytic results on both the T-Matrix and the scat-

tering length. This model captures the essence of the physics of Feshbach Resonance demonstrated in cold Fermi systems, with the advantage that the coupled-channel scattering parameters can be analytically obtained. We have discussed the different properties of broad and narrow resonances, and showed that a coupled-channel resonance can be effectively mapped to a single-channel one as long as it is broad. This result is consistent with the current understanding that the broad coupled-channel Feshbach resonances in cold Fermi gas experiments can be theoretically modeled via a single-channel formalism.

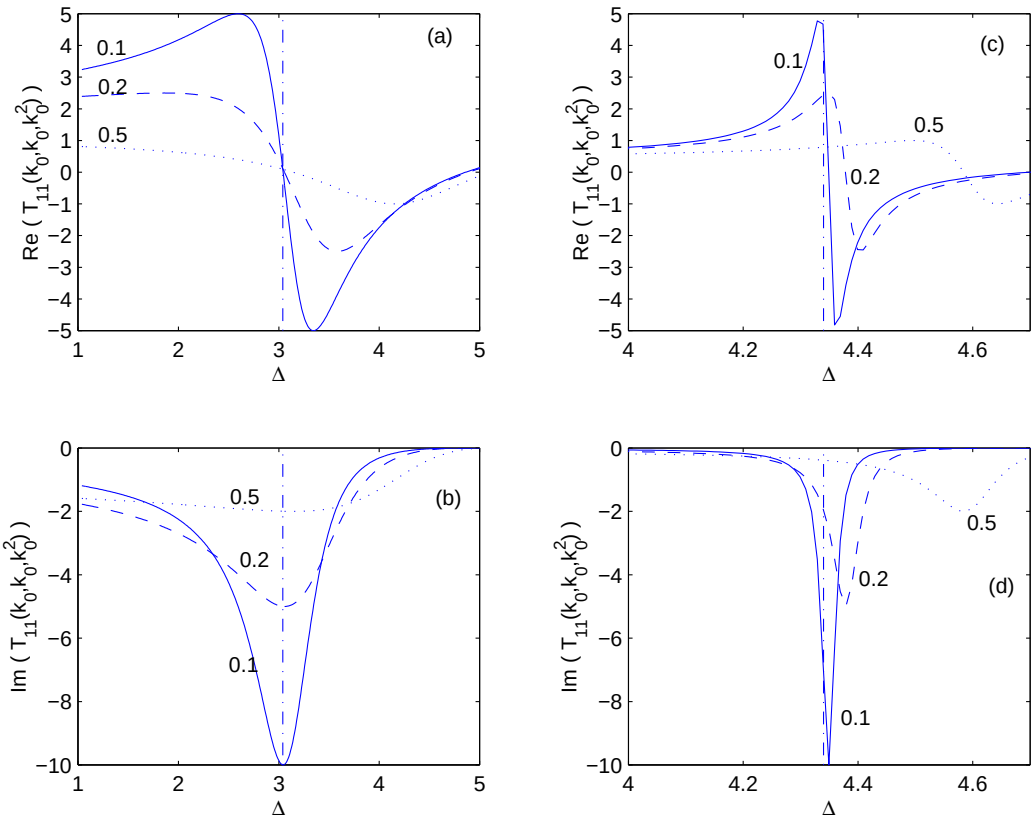

Figure 2.3: Real part and imaginary part of the on-shell T matrix element $T_{11}(k_0, k_0, k_0^2)$, with $\mu_1 = \mu 2 = \mu$, for several values of k_0. The exact position of the resonance is marked by the dash-dotted line. (a) and (b) belong to a broad resonance, with $\mu = 10.0$, $\alpha_{11} = -1.1$ $(2\mu^3)$, $\alpha_{11} = \alpha_{21} = 0.1$ α_{11}, $\alpha_{22} = -1.5$ $(2\mu^3)$. (c) and (d) belong to a narrow resonance with $\mu = 10.0$, $\alpha_{11} = -2.0$ $(2\mu^3)$, $\alpha_{11} = \alpha_{21} = 0.1$ α_{11}, $\alpha_{22} = -1.5$ $(2\mu^3)$. The solid line, dash line and dotted line refers to $k_0 = 0.1$,0.2 and 0.5 respectively.

Chapter 3

Low-momentum ring diagrams of neutron matter at and near the unitary limit

3.1 Introduction

Back in 1999, Bertsch[34] formulated a many-body problem, asking: what are the ground state properties of a two-species fermion system that has a zero-range interaction and an infinite scattering length? Such problem was originally set up as a parameter-free model for a fictitious neutron matter. At that time it was not clear whether such form of matter can be stable. Recently, as the experiments on trapped cold alkali gas undergo huge breakthroughs, degenerate Fermi gas with a tunable scattering length (including $\pm\infty$) becomes accessible in laboratories[6–8]. Since then cold Fermi systems have aroused growing attention.

As discussed in Chapter 1, many authors used the term 'unitary limit' to refer to a low-density (or small k_F) cold Fermi gas with a huge scattering length a_s. At such limit universal behavior is expected to show up in the sense that the ground state properties should be determined solely by k_F. In particular, the ground state energy, E_0, is expected to be proportional to that of the non-interacting gas E_0^{free} [15]. In other words, $E_0/E_0^{free} = \xi$, or equivalently

$$\frac{E_0}{A} = \frac{3}{5}\frac{k_F^2}{2}\xi \tag{3.1}$$

($\hbar = m = 1$) where A denotes the number of particles. The universal constant ξ is of great interest and many attempts have been made to derive it analytically or determine it experimentally.

The theoretical derivation on the value of ξ is highly challenging. In the literature one can find estimation of ξ done by researches from various fields in physics employing different many-body calculation approaches. In most of such works, ξ is between 0.3 to 0.7. For example, an early work based on different Padé approximations gives $\xi = 0.326, 0.568$[15]. Diagrammatic approach gives 0.326 with Galitskii resummation[16], 0.7 with ladder approximation[16], and 0.455 with a diagrammatic BCS-BEC crossover theory[62]. Other theoretical approaches have also been used, including ϵ expansion, which gives ξ=0.475 in [63] and [65], and variational formalism, which gives 0.360 in [64]. Cold alkali gas experimentalists have also performed measurements for obtaining ξ. The four most recent ones are listed in Table 3.1. Though the experimental results are consistent with each other, the experimentally determined value of ξ still falls between relatively large error bars($\sim$10%). By far

the best estimate on ξ is considered to be that from quantum Monte-Carlo methods. Two studies employing different underlying model potentials give highly consistent results. From Carlson *et. al.* $\xi = 0.44(1)$[38]; from Astra *et. al.* $\xi = 0.42(1)$[39].

ξ	Authors	Ref.
0.36(15)	Bourdel *el.al*	[35]
0.51(4)	Kinast *et.al.*	[32]
0.46(5)	Partridge *et.al.*	[36]
$0.46^{+0.05}_{-0.12}$	Stewart *et.al.*	[37]

Table 3.1: Comparison of recent experimental values on ξ.

Cold and dilute neutron matter is a special class of cold Fermi system with great importance in astrophysics. Its properties at resonance has attracted much interest recently [66, 67]. In this Chapter we report results from low-momentum ring diagram calculations on the ground-state energy of neutron matter at and near the unitary limit. As is well-known, the ${}^1S_0$ channel of neutron matter has a fairly large scattering length a_s (-18.97fm), nonetheless, it is still finite. Here, by adjusting the interaction parameters of the CD-Bonn potential[40], we construct 'tuned' neutron interactions with different a_s's such as -9.83fm, -12070fm and $+21$fm (which possesses a bound state). For a wide range of neutron density, the case of $a_s = -12070$fm can be considered the same as the unitary limit, namely $a_s \to -\infty$. We shall compute the ground state energy of neutron matter, with inter-neutron potentials being these 'tuned' CD-Bonn's, by two steps: renormalization followed by ring summation. We first renormalize neutron interactions with a T-matrix equivalence renormalization method [50–55], where the high-momentum com-

ponents beyond a decimation scale Λ are integrated out. This gives the corresponding low-momentum interactions V_{low-k}'s with the scattering lengths being preserved. Then, we calculate the ground state energy by summing the particle-particle-hole-hole (*pphh*) ring diagrams[68] to all orders. In such ring summation, we employ a model space approach, namely, the summation is carried out within a model space characterized by $\{k \leq \Lambda\}$.

We shall closely examine how our results differ from similar calculations with a different renormalized interaction - the Brueckner G-matrix on which the Brueckner Hartree-Fock(BHF) method is based. The BHF method has been widely used for treating the strongly interacting nuclear many body problems [69, 70]. However, BHF is a lowest-order reaction matrix (G-matrix) theory and may be improved in several aspects. To take care of the short range correlations, the ladder diagrams of two particles interacting with the bare interaction are summed to all orders in BHF. However, this method does not include diagrams representing hole-hole correlations such as diagram (iii) of Fig.3.1. Note that this diagram has repeated (*pphh*) interactions as well as self-energy insertions to both hole and particle lines. Another aspect of the traditional BHF is that it employs a discontinuous single-particle (s.p.) spectrum which has a gap at the Fermi surface k_F. To improve upon these drawbacks, Song *et al.* [68] have formulated a G-matrix ring-diagram method for nuclear matter, with which the *pphh* ring diagrams such as diagrams (i) to (iii) of Fig.3.1 are summed to all orders. This ring-diagram method has been applied to nuclear matter and given satisfactory result [68]. The V_{low-k} ring diagram method used in this Chapter is highly similar to [68]'s , except for one significant difference: the interaction used in the G-matrix ring diagram

method is energy dependent. (The Brueckner G-matrix is energy dependent, as we shall later discuss.) This complicates the calculation a lot. V_{low-k} provides a cleaner and simpler implementation on such all-order ring summation.

We shall first provide an outline of the ring-diagram approach in section 3.2. The derivation details of the low-momentum interaction from the CD-Bonn potentials shall be followed in section 3.3. Our major results from the V_{low-k} ring diagram method are in section 3.4. There we shall present our results for the ground-state energy and ratio E_0/E_0^{free} obtained with potentials of various scattering lengths. A fixed-point criterion for determining the decimation scale Λ will be discussed. There one can also find a comparison of data on the ground state energy obtained with two different methods-the V_{low-k} and the G-matrix ring diagram methods. We shall present a conclusion in the last section.

3.2 Low-momentum ring diagrams

In this section we describe how we calculate the ring diagrams for the ground state energy shift ΔE_0, which is defined as the difference $(E_0 - E_0^{free})$ where E_0 is the true ground-state energy and E_0^{free} is the corresponding quantity for the non-interacting system. In the present work, we consider the *pphh* ring diagrams as shown in Fig.3.1. We shall calculate the all-order sum, denoted as ΔE_0^{pp}, of such diagrams. Our calculation is carried out within a low-momentum model space $\{k \leq \Lambda\}$ and each vertex of the diagrams is the renormalized effective interaction corresponding to this model space. Two types of such interactions will be employed, one being the energy-independent V_{low-k} and the other being the energy-dependent G-matrix interaction. Let us

consider first the former.

To familiarize with the infinite-order ring summation, one could start with the lowest-orders terms.

$$\Delta E_0^{pp}(1) = \frac{-1}{2\pi i}\int_{-\infty}^{\infty} d\omega e^{i\omega 0^+} F_{ab}(\omega)\overline{V}_{abab}, \tag{3.2}$$

$$\Delta E_0^{pp}(2) = \frac{-1}{2\pi i}\int_{-\infty}^{\infty} d\omega e^{i\omega 0^+} \frac{1}{2} F_{ab}(\omega)\overline{V}_{abcd}F_{cd}(\omega)\overline{V}_{cdab}; \tag{3.3}$$

$$\Delta E_0^{pp}(3) = \frac{-1}{2\pi i}\int_{-\infty}^{\infty} d\omega e^{i\omega 0^+} \frac{1}{3} F_{ab}(\omega)\overline{V}_{abcd}F_{cd}(\omega)\overline{V}_{cdef}F_{ef}(\omega)\overline{V}_{efab}; \tag{3.4}$$

where repeated indices are summed over and F is the free *pphh* propagator

$$F_{ab}(\omega) = \frac{\bar{n}_a\bar{n}_b}{\omega - (\epsilon_a + \epsilon_b) + i0^+} - \frac{n_a n_b}{\omega - (\epsilon_a + \epsilon_b) - i0^+} \tag{3.5}$$

with

$$n_a = 1,\ a \leq k_F;\ \ = 0,\ k > k_F \qquad \bar{n}_a = (1 - n_a). \tag{3.6}$$

In the above we used $\overline{V}$ to denote an anti-symmetrized matrix element, namely $\overline{V}_{abcd} = \frac{1}{2}\left(V_{abcd} - V_{abdc}\right)$. Notice that within our model space treatment, the summation over the single-particles states are restricted for states *inside* the chosen model space only.

One can now write down an expression for an all-order sum of similar ring diagrams, giving [68]

$$\begin{aligned}\Delta E_0^{pp} = \frac{-1}{2\pi i}\int_{-\infty}^{\infty} d\omega e^{i\omega 0^+} tr_{<\Lambda}[F(\omega)V_{low-k} \\ + \frac{1}{2}(F(\omega)V_{low-k})^2 + \frac{1}{3}(F(\omega)V_{low-k})^3 + \cdots]\end{aligned} \tag{3.7}$$

Let us introduce a strength parameter λ and a λ-dependent Green function $G^{pp}(\omega, \lambda)$ defined by

$$G^{pp}(\omega, \lambda) = F(\omega) + \lambda F(\omega) V_{low-k} G^{pp}(\omega, \lambda). \tag{3.8}$$

The energy shift then takes the following simple form when expressed in terms of G^{pp}, namely

$$\Delta E_0^{pp} = \frac{-1}{2\pi i} \int_0^1 d\lambda \int_{-\infty}^{\infty} e^{i\omega 0^+} tr_{<\Lambda}[G^{pp}(\omega, \lambda) V_{low-k}] \tag{3.9}$$

A convenient way to proceed is to make use of the Lehmann's representation for G^{pp} where it is expressed in terms of the transition amplitudes X's and Y's. One can show that

$$\Delta E_0^{pp} = \int_0^1 d\lambda \Sigma_m \Sigma_{ijkl<\Lambda} Y_m(ij, \lambda) Y_m^*(kl, \lambda) \langle ij | V_{low-k} | kl \rangle, \tag{3.10}$$

where the transition amplitudes Y are given by the following RPA equation:

$$\begin{aligned} &\sum_{ef} [(\epsilon_i + \epsilon_j)\delta_{ij,ef} + \lambda(1 - n_i - n_j)\langle ij | V_{low-k} | ef \rangle] \\ &\times Y_m(ef, \lambda) = \omega_m Y_m(ij, \lambda); \quad (i, j, e, f) < \Lambda. \end{aligned} \tag{3.11}$$

The index m denotes states dominated by hole-hole components, namely, states that satisfy $\langle Y_m | \frac{1}{Q} | Y_m \rangle = -1$ and $Q(i, j) = (1 - n_i - n_j)$. We have

used the HF s.p. spectrum given by V_{low-k}, namely

$$\epsilon_k = \frac{k^2}{2} + \sum_{h<k_F} \langle kh|V_{low-k}|kh\rangle \tag{3.12}$$

for both holes and particles with $k \leq \Lambda$. Thus the propagators of the diagrams as shown in Fig.3.1 all include HF insertions to all orders. The above spectrum is continuous up to Λ.

The above ring-diagram method is a renormalization group approach for a momentum model space defined by a momentum boundary Λ, and the space with momentum greater than Λ is integrated out. The resulting effective interaction for the model space is V_{low-k} which is energy independent. This renormalization procedure can, however, also lead to a model-space effective interaction which is energy dependent. The G-matrix ring-diagram method of [68] is of the latter approach. Formally, these two approaches should be the same. In the present work we shall carry out ring-diagram calculations using both approaches; it would be of interest to compare the results of these two different approaches.

In the following, let us briefly describe the G-matrix ring diagram method [68]. Here each vertex of Fig.3.1 is a model-space G-matrix interaction, to be denoted as G^M. It is defined by

$$G^M_{ijkl}(\omega) = V_{ijkl} + \sum_{rs} V_{ijrs} \frac{Q^M(rs)}{\omega - \epsilon_r - \epsilon_s + i0^+} G^M_{rskl}(\omega). \tag{3.13}$$

The Pauli projection operator Q^M is to assure the intermediate states being

outside Λ and k_F, namely it is defined by

$$\begin{aligned} Q^M(rs) &= 1, if\ max(k_r, k_s) > \Lambda\ and\ min(k_r, k_s) < k_F \\ &= 0, otherwise. \end{aligned} \tag{3.14}$$

In the above $k_F < \Lambda$. In Ref.[68] Λ is chosen to be $\sim 3\text{fm}^{-1}$. Note that the above G^M is energy dependent, namely it is dependent on the energy variable ω. However, ω is not a free parameter; it is to be determined in a self-consistent way. For example, the model-space s.p. spectrum is given by the following self-consistent equations:

$$\epsilon_a = \frac{k_a^2}{2} + \langle a|U|a\rangle; \tag{3.15}$$

$$\begin{aligned} \langle a|U|a\rangle &= \sum_{h \le k_F} \langle a,h|G^M(\omega = \epsilon_a + \epsilon_h)|a,h\rangle,\ a < \Lambda \\ &= 0,\ otherwise. \end{aligned} \tag{3.16}$$

In the above U is the s.p. potential and ϵ the model-space s.p. energy which is determined self-consistently with the energy variable of G^M. Note that this s.p. spectrum does not have a gap at k_F; it is a continuous one up to Λ. When choosing Λ=k_F the above is the same as the self-consistent BHF s.p. spectrum.

When calculating the ring diagrams using G^M, its energy variable is also determined self-consistently. In terms of G^M, the all-order sum of the *pphh*

ring diagrams is [68]

$$\Delta E_0^{pp} = \int_0^1 d\lambda \sum_m \sum_{ijkl(<\Lambda)} Y_m(ij,\lambda) Y_m^*(kl,\lambda) G^M_{kl,ij}(\omega_m^-) \tag{3.17}$$

where the transition amplitudes Y_m and eigenvalues ω_m^- are given by the following self-consistent RPA equation:

$$\begin{aligned} &\sum_{ef}[(\epsilon_i+\epsilon_j)\delta_{ij,ef} + \lambda(1-n_i-n_j)L_{ij,ef}(\omega)]Y_m(ef,\lambda) \\ &= \mu_m(\omega,\lambda)Y_m(ij,\lambda); \quad (i,j,e,f) < \Lambda. \end{aligned} \tag{3.18}$$

The index m denotes states dominated by hole-hole components. The vertex function L is obtained from 2- and 1-body diagrams first order in G^M [68]. The above equation is solved with the self-consistent condition that the energy variable of L is equal to the eigenvalue, namely

$$\omega = \mu_m(\omega,\lambda) \equiv \omega_m^-(\lambda). \tag{3.19}$$

Comparing with the V_{low-k} ring diagram calculation described earlier, the above G-matrix calculation is clearly more complicated. Because of the energy dependence of the interaction G^M, the above equations have to be solved self-consistently both for the s.p. spectrum and for the RPA equations. To attain this self consistency, it is necessary to use iteration methods and this procedure is often numerically involved. In contrast, ring-diagram calculation using the energy-independent interaction V_{low-k} is indeed much simpler. As mentioned earlier, we shall carry out ring-diagram calculations using both methods.

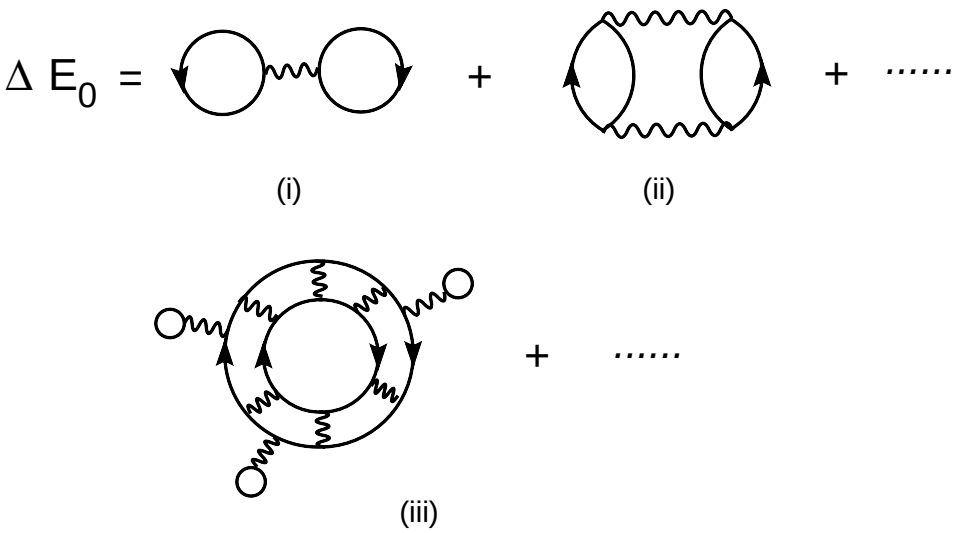

Figure 3.1: *pphh* ring-diagram summation in the calculation of the ground state energy shift.

3.3 V_{low-k} with infinite scattering length

To carry out the above ring-diagram calculation, we need the low-momentum potential V_{low-k}. Since we are interested at neutron matter at and near the unitary limit (infinite scattering length), we should have V_{low-k}'s of definite scattering lengths, including $\pm\infty$, so that the dependence of our results on scattering lengths can be investigated. In the present work, we have chosen a two-step procedure to construct such potentials so that the resulting potentials are close to realistic neutron potentials. We first construct bare potentials V^a based on a realistic nucleon-nucleon potential; these potentials are tuned so that they have definite scattering lengths. Renormalized low-momentum potentials V^a_{low-k} are then obtained from V^a using a renormalization procedure which preserves the scattering length.

We start from the high-precision CD-Bonn [40] nucleon-nucleon potential.

For this potential, the scattering length of the $^1S_0$ channel is already fairly large (-18.97 fm), and it is found to depend rather sensitively on the interaction parameters. Thus by slightly tuning the interaction parameters of the CD-Bonn potential, we have obtained a family of $^1S_0$ neutron potentials of definite scattering lengths. We shall denote them as V^a. Our tuning procedure will be discussed in section 3.4.1.

Recently there have been a number of studies on the low-momentum nucleon-nucleon potential V_{low-k} [50–55]. V_{low-k} is obtained from a bare nucleon-nucleon potential by integrating out the high-momentum components, under the restriction that the deuteron binding energy and the low-energy phase-shifts are preserved. The V_{low-k} obtained from different realistic potentials (CD-Bonn [40], Argonne [47] , Nijmegen [48] and Idaho [49]) all flow to a unique potential when the cut-off momentum is lowered to around 2fm^{-1}. The above V_{low-k} is obtained using a T-matrix equivalence renormalization procedure [50–55]. Since this procedure preserves the half-on-shell T-matrix, it of course preserves the scattering length. Thus this procedure is suitable for constructing V^a_{low-k}, the low-momentum interaction with definite scattering length. Using this procedure, we start from the T-matrix equation

$$T(k', k, k^2) = V^a(k', k) + \int_0^\infty q^2 dq \frac{V^a(k', q)T(q, k, k^2)}{k^2 - q^2 + i0^+}, \tag{3.20}$$

where V^a is a modified CD-Bonn potential of scattering length a. Notice that in the above the intermediate state momentum q is integrated from 0 to ∞.

We then define an effective low-momentum T-matrix by

$$\begin{aligned} T_{low-k}(p', p, p^2) &= V^a_{low-k}(p', p) \\ &+ \int_0^\Lambda q^2 dq \frac{V^a_{low-k}(p', q) T_{low-k}(q, p, p^2)}{p^2 - q^2 + i0^+}, \end{aligned} \tag{3.21}$$

where the intermediate state momentum is integrated from 0 to Λ, the momentum space cut-off. We require the above T-matrices to satisfy the condition

$$T(p', p, p^2) = T_{low-k}(p', p, p^2);\ (p', p) \leq \Lambda. \tag{3.22}$$

The above equations define the effective low momentum interaction V^a_{low-k}. The iteration method of Lee-Suzuki-Andreozzi [71, 72] has been used in calculating V^a_{low-k} from the above T-matrix equivalence equations. From now on, we shall denote V^a_{low-k} simply as V_{low-k}.

3.4 Results

3.4.1 Low-momentum interactions and scattering lengths

To study neutron matter at the unitary limit, we first need a realistic neutron-neutron interaction that would lead to a huge $^1S_0$ scattering length a_s, and a small effective range r_e. We obtain such interaction by 'tuning' the meson mass m_σ in the usual CD-Bonn potential. The exchange of a lighter meson generates a stronger attraction, therefore making the scattering length a_s more negative until a bound state is formed. As one 'tunes' across the bound state,

name	$m_\sigma(MeV)$	a_s(fm)	r_e(fm)
original CD-Bonn	452	-18.97	2.82
CD-Bonn-10	460	-9.827	3.11
CD-Bonn-42	447	-42.52	2.66
CD-Bonn-∞	442.85	-12070.00	2.54
CD-Bonn+∞	442.80	+5121.00	2.54
CD-Bonn+21	434	+21.01	2.31

Table 3.2: m_σ in the original CD-Bonn potential is tuned to give neutron-neutron potentials with different scattering lengths.

a_s will pass from $-\infty$ to $+\infty$, eventually become less and less positive. In this work, this m_σ 'tuning' is taken as a manual adjustment in the strength of the neutron-neutron potential. Of great interest is that this 'tuning' may naturally come from the density-dependence of the nucleon-nucleon potential via the mechanism of Brown-Rho (BR) scaling[42, 43, 73], which suggests the in-medium meson masses should *decrease*.

At normal nuclear matter density, the meson masses of ρ, ω and σ are all expected to decrease by about 15% [73] compared to their masses in free space. This decrease will enhance not only the attraction from σ but also the repulsion from ρ and ω. As a preliminary study, we shall tune only m_σ in the present work. To compensate for the repulsive effect from ρ and ω (which are not tuned in the present work), we shall only tune m_σ slightly, namely a few percent. We shall consider that the above BR scaling is compatible with neutron matter of moderate density ($k_F \sim 1\text{fm}^{-1}$).

Various 'tuned' CD-Bonn potentials are listed in Table 3.2. From there one can see the sensitivity of the scattering length to the change in m_σ. At $m_\sigma \approx 442MeV$, namely a 2.4% decrease from the original, $a_s \approx -12000$fm. Notice

that the effective ranges for the CD-Bonn potentials are larger than the actual ranges of them. For example, r_e for the original CD-Bonn potential is 2.82fm, considerably larger than the range of one-pion exchange. Within the range of Fermi momenta from 0.8fm^{-1} to 1.5fm^{-1} that we use in our computation below, $a_s \approx -12000$fm is obviously enormous compared to any length scale in the system, thus we expect the neutron matter to be at the unitary limit, i.e., no different from the limiting case $a_s = -\infty$. For convenience, we name such potential CD-Bonn-∞.

Following the renormalization procedures as already described in section 3.3, we obtain the low-momentum potential V_{low-k}'s for several CD-Bonn potentials listed above. A comparison of the diagonal matrix elements in the V_{low-k}'s (with a fixed cut-off momentum Λ) is shown in Fig.3.2. It is of interest that the strength of V_{low-k} only changes weakly with the scattering length. For example, it changes by merely about 10% from $a_s = -18.97$fm to -12070fm.

3.4.2 Ground-state energy and the universal constant ξ

Here we shall present our major results, namely the ground state energies E_0 of neutron matter at and close to the unitary limit from the summation of low-momentum ring diagrams to all orders. Following the potential renormalization procedure described in section 3.3, we first calculate V_{low-k} for certain chosen values for the decimation scale Λ. Then the all-order sum of the *pphh* ring diagrams are calculated using the above V_{low-k}. In the actual numerical computation, Eqn. 3.10 is treated in the relative and center-of-mass frame.

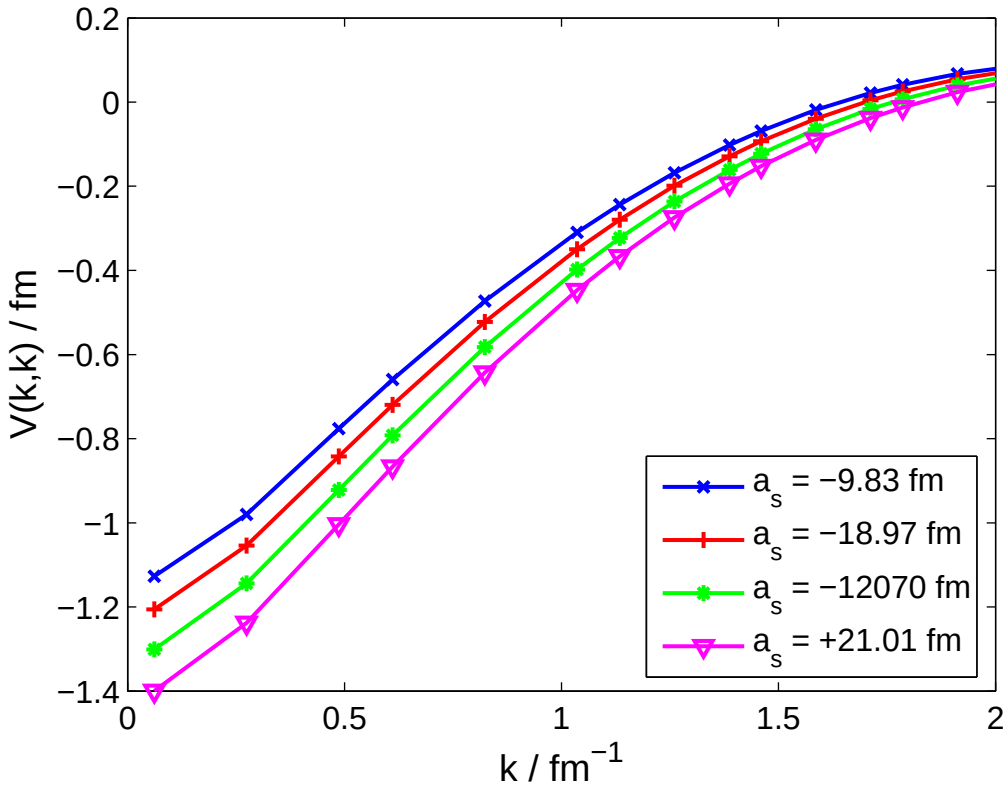

Figure 3.2: Diagonal matrix elements of V_{low-k} constructed from CD-Bonn potentials with different scattering lengths. $\Lambda = 2.4\text{fm}^{-1}$ is used in all cases.

The final expression, in terms of the relative and center-of-mass coordinates, for the ground state energy shift is

$$\frac{\Delta E^{PP}}{A} = \frac{6}{\pi^2 k_F^3}\int_0^1 \mathrm{d}\lambda \sum_m \int_0^{2\Lambda} \mathrm{d}K K^2 \int_0^{\Lambda} \mathrm{d}k_1\, k_1^2 \int_0^{\Lambda} \mathrm{d}k_2\, k_2^2 \; Y_m^*(k_1, K\lambda) Y_m(k_2, K\lambda) V_{low-k}(k_1 k_2, K\lambda). \tag{3.23}$$

In the above, k_1 and k_2 are relative momenta while K is the center-of-mass momentum. In our calculation only the contribution from $^1S_0$ channel is included.

How to choose the decimation scale Λ is clearly an important step in our calculation, and in the present work we shall use a stable-point, or 'fixed-point', criterion in deciding Λ. Before discussing this criterion, let us first present some of our results for the ground-state energy per particle (E_0/A). In Fig.3.3 we present such results for four a_s values, calculated with Λs determined by the above criterion. (The details of this determination will be described a little later.) As shown by the figure, we see that E_0/A does not change strongly with a_s. The ratios $\xi = E_0/E_0^{free}$ are then readily obtained, as shown in Fig.3.4. It is of interest that the ratios for the four a_s cases are all weakly dependent on k_F. To help understand this behavior, we plot in Fig.3.5 the potential energy per particle PE/A (namely $\Delta E_0^{pp}/A$ of Eqn.3.23) versus k_F^2, for the same four a_s cases. It is rather impressive that they all appear to be straight lines. We have fitted the 'lines' in the figure to the equation

$$\frac{PE}{A} = \beta k_F^2 + \gamma \tag{3.24}$$

We have found (β, γ) =(-0.1370, 0.0002), (-0.1498, -0.0008), (-0.1649, -0.0035) and (-0.1797, -0.0082) respectively for $a_s = -9.87$fm, -18.97fm, -12070fm and $+21.0$fm. The rms deviation for the above fitting are all very small (all less than 0.0013), confirming that they are indeed very close to straight lines. The above results are of interest, and are consistent with those shown in Fig.3.4. In fact the ratios of Fig.3.4 are determined by the 'slopes' of these 'lines'.

Before further discussing our results, let us now address the question of how to determine the decimation scale Λ. There are basically two considerations: The first one concerns the experimental NN scattering phase shifts on

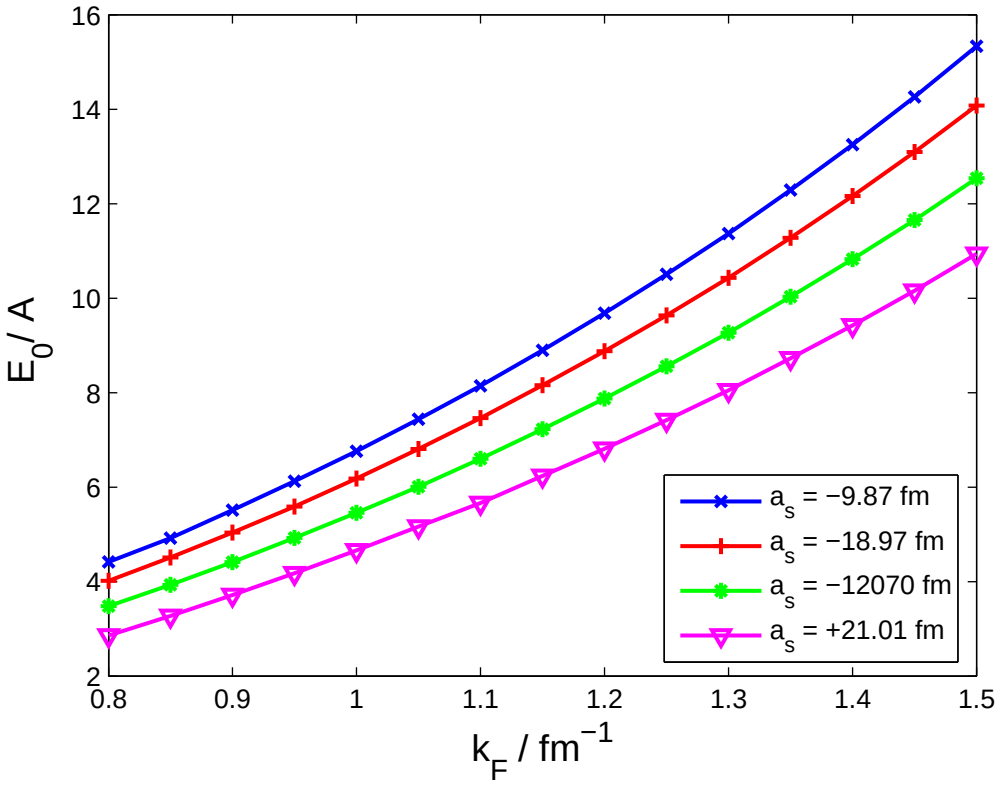

Figure 3.3: Ground state energy per particle, E_0/A, of neutron matter with various tuned CD-Bonn potentials, computed from the summation of low-momentum *pphh* ring diagrams. Only $^1S_0$ contribution is included.

which realistic NN potentials are based. The second is about the dependence of our results on Λ. Realistic NN potentials [40, 47–49] are constructed to reproduce the experimental NN phase shifts up to $E_{lab} \approx 300 MeV$. This suggests that Λ is about 2fm^{-1}, as beyond this scale NN potential models are not experimentally constrained and are thus rather uncertain (model dependent) [54].

Our V_{low-k} contains the effects of short-range correlations by including the ladder diagrams between a pair of particles to all orders. Then, in summing up

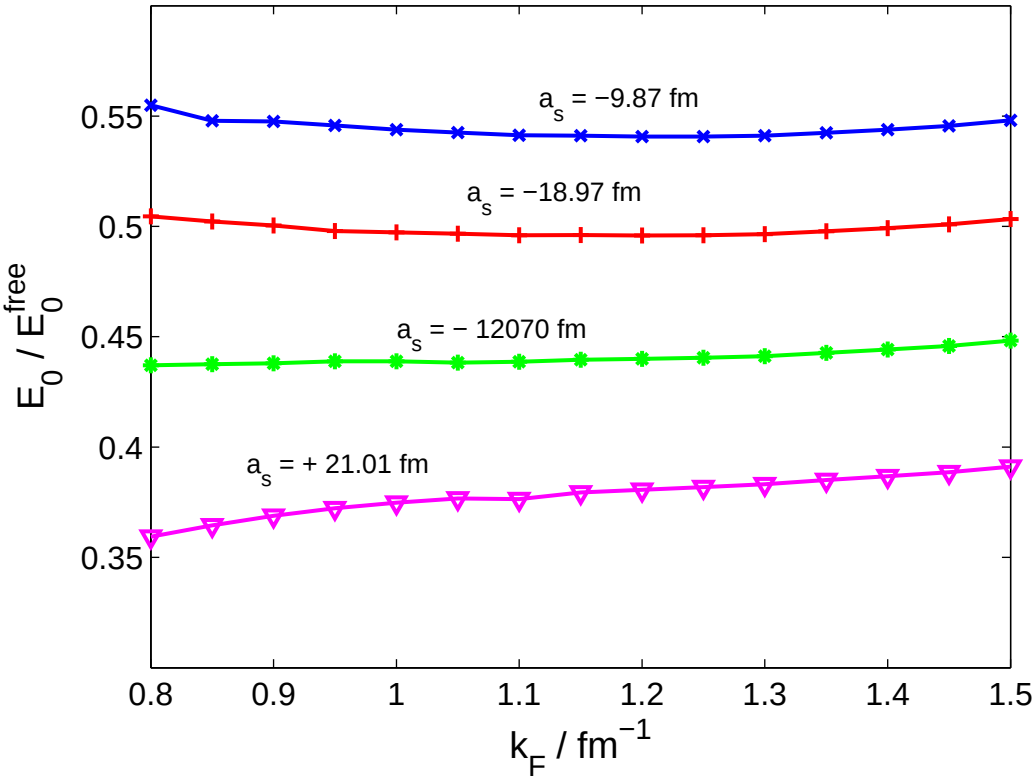

Figure 3.4: The ratio E_0/E_0^{free} as a function of Fermi momentum k_F for the various CD-Bonn potentials listed in Table 3.2. The data with CD-Boon-$\infty(a_s = -12070\text{fm})$ indicates that E_0/E_0^{free} is a constant of 0.443 ± 0.006 over the range of k_F as shown.

the *pphh* ring diagrams to all orders in a model-space ($k < \Lambda$), the long-range correlations corresponding to low-energy fluctuations of the Fermi surface are also taken care of. In doing so, we must allow enough 'particle-space' for the $p-h$ excitations to take place. Thus Λ needs to be sufficiently larger than k_F. The above considerations suggests that Λ has a lower bound $> k_F$ and an upper bound near 2fm^{-1}.

We now turn to the dependence of our results on Λ. As described in section 3.2, V_{low-k} is used in the determination of the H.F. single particle

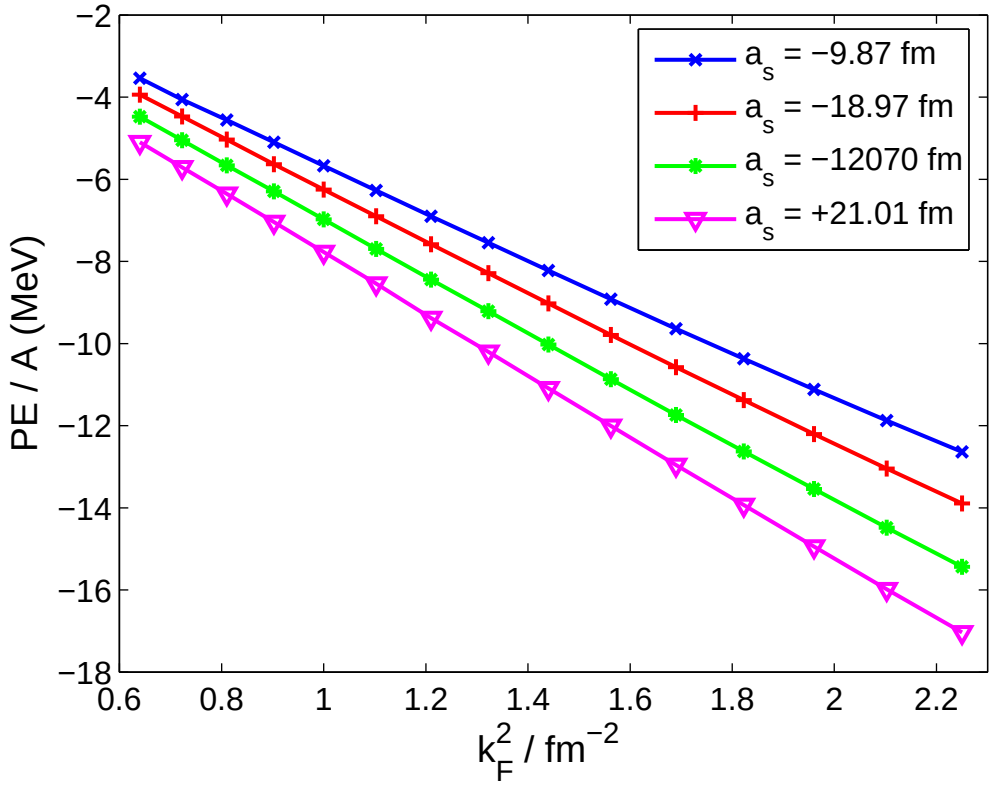

Figure 3.5: Potential energy per particle, PE/A, of neutron matter with various tuned CD-Bonn potentials, computed from the summation of low-momentum *pphh* ring diagrams. Only $^1S_0$ contribution is included.

spectrum (see Eqn.5.22), the transition amplitudes Y in the RPA equation (see Eqn.3.11), and finally, the ground state energy E_0 (see Eqn.3.10). Intuitively, E_0 should exhibit a non-trivial Λ-dependence. For various Fermi-momenta, this dependence is studied and is found to be remarkably mild.

As an example, let us present in Fig.3.6 our results obtained with the potential CD-Bonn-∞. For $\Lambda = (2.0 - 2.6)\text{fm}^{-1}$, it is seen that ξ varies actually by a rather small amount (note that the range of our plot is from 0.438 to 0.444). Furthermore the Λ dependence of ξ shows up as a curve with

a minimum. The final choice of Λ is based on the criterion that E_0 should be stable against changes in Λ. As shown in the figure, an obvious stable-point, or fixed-point, defined by $dE_0(\Lambda)/d\Lambda = 0$, is found at about 2.3fm^{-1}. Thus we have used $\Lambda = 2.3\text{fm}^{-1}$ for CD-Bonn-∞. We found that the position of the fixed point is almost the same for the different Fermi-momenta in the range $(0.8 - 1.5)\text{fm}^{-1}$. The same procedure is done on the original CD-Bonn, and other tuned potentials. The fixed points, also with an negligible dependence on k_F, are found to be 2.15fm^{-1}, 2.25fm^{-1} and 2.4fm^{-1} respectively for CD-Bonn potentials of scattering lengths -9.8fm, -18.9fm (the original CD-Bonn), and $+21.01$fm. The above fixed-point Λ's have been used for the results presented in Figs.3.3-3.5.

Of great significance is the ratio of the ground state energy to that of the non-interacting case, namely E_0/E_0^{free}. At the unitary limit, it is expected to be an universal constant, named ξ. This constant is of great importance as it determines the equation of state of all low-density cold Fermi gas. At the unitary limit, our data on E_0/E_0^{free} all lie within a narrow window from 0.437 to 0.448. Such result confirms a universality over Fermion density in a wide range $(1.73 - 11.40) \times 10^{-2}\text{fm}^{-3}$. Most importantly, the numerical value of ξ is remarkably close to that from Monte Carlo methods, which by far is believed to be the best estimate. Astra *et. al.* obtained 0.42(1) based on a square well potential and particle density $nR_0^3 = 10^{-6}$ (where R_0 is the potential range). Carlson *et. al.* obtained 0.44(1) based on a 'cosh potential', and particle density $n\mu^{-3} = 0.020$ (where $2/\mu$ is the effective range). In our case, $n\Lambda^{-3} = (1.4 - 9.4) \times 10^{-3}$ (where $\Lambda = 2.3\text{fm}^{-1}$ is the decimation scale in the renormalization). These works, including ours, employ very different

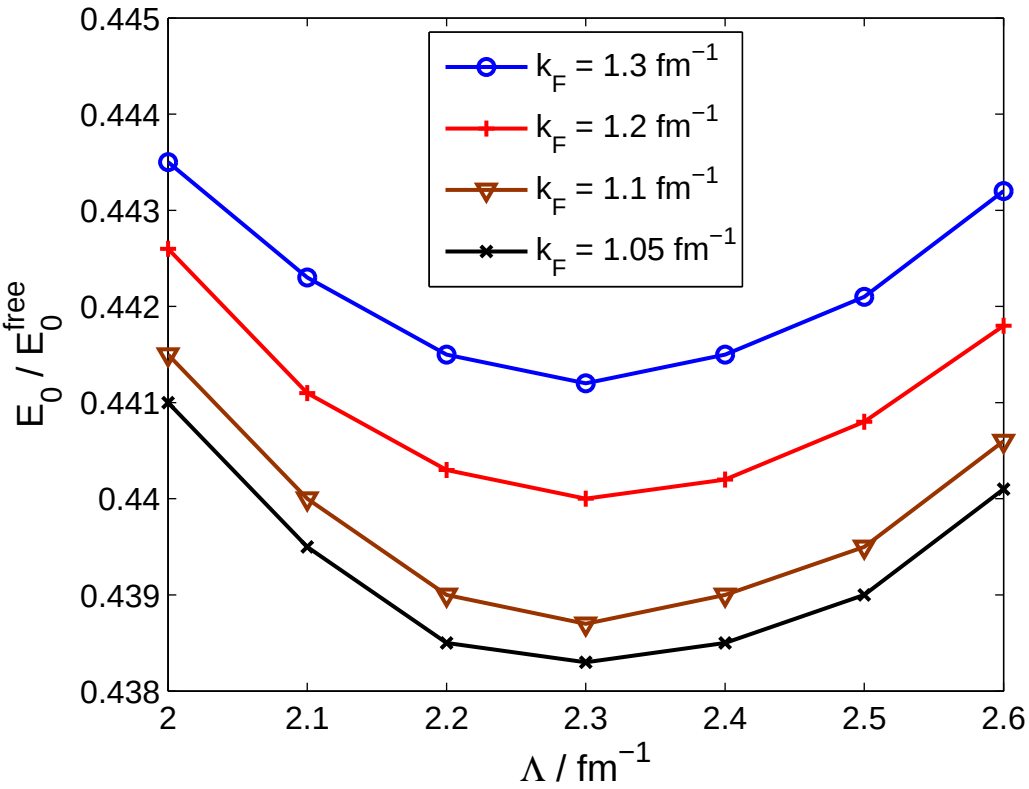

Figure 3.6: Determination of the fixed point where $dE_0/d\Lambda = 0$ for CD-Bonn-∞.

interactions and various particle densities. Still, the value of ξ agrees incredibly well.

In Fig.3.4 we contrast the data from CD-Bonn-∞ with that from the original CD-Bonn and other tuned potentials. Even though the $^1S_0$ scattering length in the original CD-Bonn is already fairly large ($a_s = -18.97$fm) , still the equation of state, as predicted from the ratio E_0/E_0^{free}, has significant difference from the unitary limit. As seen in our data with CD-Bonn-∞ potential, at the unitary limit the ratio $E_0/E_0^{free} = 0.44$ is practically independent of the underlying neutron density n.

3.4.3 Comparison with G-matrix results

As discussed in section 3.2, our ring-diagram calculations are based on a model space framework. A model-space is defined by momentum $\{k \leq \Lambda\}$ where Λ is the decimation scale. The space with $k > \Lambda$ is integrated out, resulting in a model-space effective interaction V_{eff}. We have used so far the energy-independent V_{low-k} for V_{eff}. Alternatively, on can also use the energy-dependent G^M-matrix (of section 3.2) as V_{eff}. These two approaches are formally equivalent. We have carried out calculations to check this equivalence.

We have repeated the ring diagram summation with the energy-independent V_{low-k} replaced by the energy-dependent model-space Brueckner G^M-matrix, and carry out a fully self-consistent computation in summing up the *pphh* ring diagrams. The exact procedures in Ref.[68] are followed (section 3.2). Ring diagrams within a model space up to a cut-off momentum Λ is summed to all orders. We found that the ground state energy is rather insensitive to the choice of Λ. See Fig.3.7 for the data of CD-Bonn-∞ and CD-Bonn(-18.97), done with $\Lambda = 2.3\text{fm}^{-1}$, 2.25fm^{-1} respectively. As illustrated, the two methods, namely, ring diagram summation with V_{low-k} and that with G^M-matrix, are fully consistent. This is a remarkable and reassuring result, as the calculational procedures of them are vastly different. For the G^M case, the s.p. spectrum, the RPA amplitudes Y and energies ω_m^- are all calculated self-consistently, while for the V_{low-k} case no such self-consistent procedures are needed. Clearly the V_{low-k} ring-diagram method is more desirable.

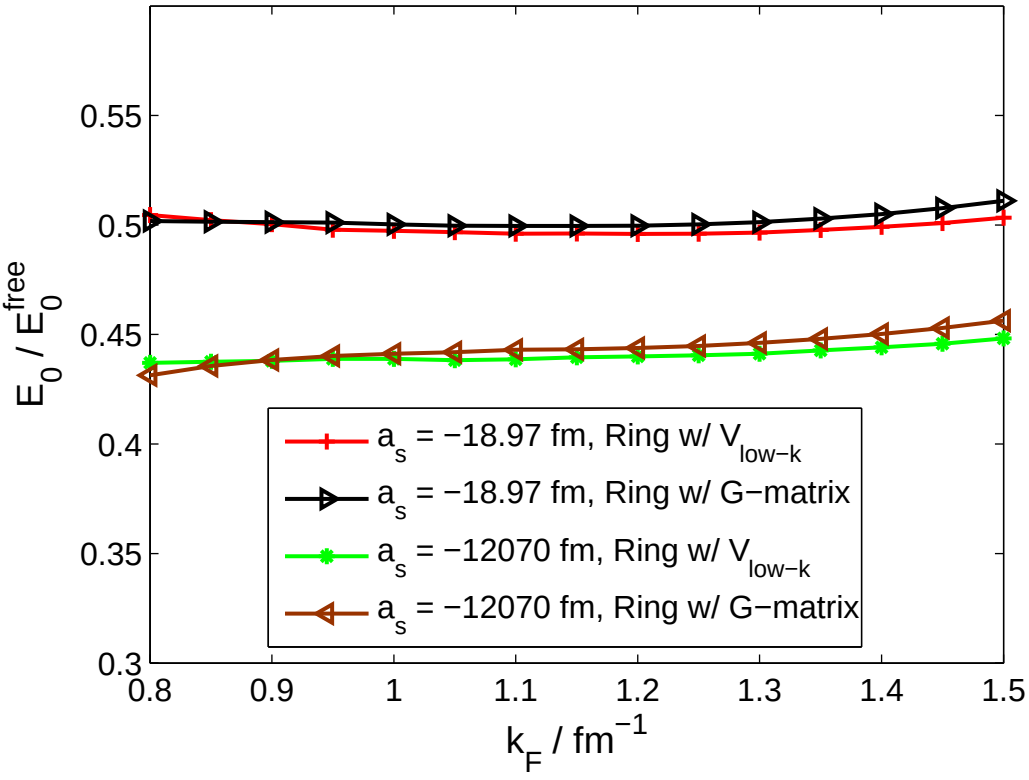

Figure 3.7: The ratio E_0/E_0^{free} for the potentials CD-Bonn-∞ and CD-Bonn(-19.87) computed with two methods. Ring w/ G-mat: *pphh* ring diagrams summation with Brueckner G^M-matrix. $\Lambda = 2.3\text{fm}^{-1}$ is used, computation is fully self-consistent. Ring w/ V_{low-k}: *pphh* ring diagrams summation with V_{low-k}, fixed point is at $\Lambda = 2.3$.

3.4.4 Schematic effective interaction at unitary limit

At the unitary limit, the simple equation of state $E_0 = \xi E_0^{free}$ in neutron matter suggests a very counter-intuitive nature in the underlying system: strongly interacting fermions essentially can be described by a non-interacting picture with an effective mass. This unexpected 'simplicity' can best be captured by a schematic interaction. To illustrate this, let us consider neutron matter confined in a closed Fermi sea $|\Phi_0(k_F)\rangle$. In other words, we consider neutron

matter in a one-dimensional model space. We denote the effective interaction for this model space as V_{FS}. Then the potential energy per particle is

$$\begin{aligned} \frac{PE}{A} &= \langle \Phi_0(k_F)|V_{FS}|\Phi_0(k_f)\rangle/A \\ &= \frac{8}{\pi}\int_0^{k_F}\left(1-\frac{3k}{2k_F}+\frac{k^3}{2k_F^3}\right)\langle k|V_{FS}|k\rangle k^2 \mathrm{d}k \end{aligned} \tag{3.25}$$

where k is the relative momentum.

Suppose we take V_{FS} as a contact effective interaction

$$V_{FS} = \frac{1}{\frac{S}{a_s}-\frac{2}{\pi}k_F} \tag{3.26}$$

($\hbar = m = 1$) where S is a positive parameter with $S \ll |a_s|$. When S=1 and k_F replaced by Λ, V_{FS} is the same the effective interaction for the pion-less effective field theory [54, 92]. Substituting the above into Eqn.3.25 gives

$$\xi = 1+\frac{5}{9}\frac{1}{\frac{\pi}{2}\frac{S}{a_s k_F}-1}. \tag{3.27}$$

At the unitary limit (infinite a_s), the above gives ξ=4/9, independent of k_F, which is practically the same as the result for ξ(-12070) of Fig.3.4. The above also gives ξ for finite a_s. At the unitary limit, we expect V_{FS} to be unique. For finite a_s (away from the unitary limit), it is not expected to be unique and the parameter S is expected to depend on the underlying potential. As shown in Fig.3.4, we have calculated ξ using the CD-Bonn potentials of finite scattering lengths. These results can also be qualitatively described by the above equation. For instance, for $S = 1.25$ and $k_F = 1.0$, the above

equation gives ξ= 0.54, 0.50 and 0.39 respectively for a_s=−9.87fm, −18.97fm and +21.01fm. In short, certain main features of our results obtained from ring-diagram calculations with the CD-Bonn potentials can be qualitatively reproduced by the above simple contact effective interaction.

3.5 Conclusion

We have carried out a detailed study on neutron matter at and close to the unitary limit with a low-momentum ring diagram approach. By slightly tuning the realistic CD-Bonn potential, we have obtained $^1S_0$ neutron potentials of specific scattering lengths, in particular the CD-Bonn-∞ giving a_s of −12070fm. By integrating out the high-momentum components beyond a decimation scale Λ, we obtain renormalized low-momentum interactions V_{low-k} for the corresponding tuned potentials. The ground state energy E_0 of neutron matter are then calculated by summing up the *pphh* ring diagrams to all orders within the model space $\{k < \Lambda\}$. A fixed-point criterion is used to determine the decimation scale Λ. V_{low-k} is energy- independent, similar calculations employing another renormalized interaction, namely the energy-dependent G-matrix, give almost identical results. The V_{low-k} ring-diagram method has a simpler formalism and is also more suitable for numerical calculation. For the CD-Bonn-∞ potential, the ratio E_0/E_0^{free} is found to be almost a constant of 0.44 over the neutron density range $(1.73 - 11.40) \times 10^{-2}\text{fm}^{-3}$. Our result agrees well with the recent experimental measurement and Monte-Carlo computation on cold Fermi gas at the unitary limit.

Chapter 4

Renormalized atomic interaction and quadrupole excitations of cold Fermi gas near Feshbach resonance

4.1 Introduction

Elementary excitations has served as a powerful tool for probing fundamental properties of cold quantum gas, especially fermionic ones. As mentioned in earlier Chapters, in cold alkali gas experiments the effective atomic interactions can be controlled via the mechanism of Feshbach resonance[6–8]. As the atomic attraction is tuned up trapped cold Fermi gas can be made to undergo a BCS-BEC crossover meaning the wavefunction of the system evolves smoothly from the BCS-type to the BEC-type[4, 5]. Accompanied with such a crossover is a

change in collision dynamics and the overall equation of state. Measurements of low-lying collective excitations can enrich our understanding of the crossover from these aspects.

To understand the experimental results of collective excitations in trapped cold alkali gas one must start with the geometry of the traps. They are elongated with cylindrical symmetry, namely of a cigar shape. Apart from the simple sloshing modes (center-of-mass oscillations), there are three elementary collective modes: one axial mode and two radial modes. The *axial mode* corresponds to an oscillation of the length of the 'cigar'. The *radial breathing mode* is a compression mode associated with an oscillation of the radius of the 'cigar'. Finally, the *radial quadrupole mode* is a pure surface oscillations. See, for example, Ref.[74] for details for these excitation modes.

In order to predict the frequency of the above excitations, it is necessary to identify two distinct regimes throughout the BCS-BEC crossover. The *collisionless* regime, as the name suggested, represents the collision-suppressed dynamics in a weakly interacting degenerate Fermi gas at low temperature. The suppression of elastic collision is a result of Pauli blocking, since elastic scattering will not be possible if the final state is already occupied. The oscillations frequencies are essentially determined by the trap frequency. The *hydrodynamic* regime refers to the either the superfluid hydrodynamic behavior expected in a strongly interacting cold Fermi gas below the critical temperature, or the usual collisional hydrodynamic behavior above that. Collective mode frequencies must be solved based on the hydrodynamical equation of motion. A good review of related theories can be found in Ref. [75]. It is worth pointing out that, both below and above the critical temperature

strongly interacting cold Fermi gas obey the same hydrodynamic equations, therefore observation of hydrodynamic behavior in experiment cannot by itself distinguishes between the two.

Collective excitations of trapped cold alkali gas has been measured. Close to the Feshbach resonance, the measured frequency of the radial compression mode is in excellent agreement with that from a superfluid hydrodynamic theory[22, 26]. However, at a magnetic field greater than the resonance position, namely, on the BCS-side of the resonance, a sharp increase in frequency accompanied with a large decay rate is observed, signalling a 'breakdown' of the hydrodynamic regime. Similar 'breakdown' was also observed in the radial quadrupole mode [27], but not in the axial mode[25]. These experimental findings suggest interesting physics as a cold Fermi gas 'transits' from the hydrodynamic to the collisionless regime. Intuitively, as the system 'enters' the collisionless regime an increase in relaxation time is expected owing to the suppression of collisions. An accurate theoretical determination of the damping rate is still the subject of current research (see Ref. [76] and references therein).

Motivated by the above experiments, we have carried out a *microscopic* study for the quadrupole excitations of a model trapped cold Fermi gas at zero-temperature, aiming primarily at the transitional and collisionless regimes. We shall use a particle-hole Green's function framework which has been commonly used in nuclear physics [77–79]. When applying this method to nuclear systems, nucleons are placed in an oscillator well and particle-hole excitations are treated to all orders using either the Tamm-Dancoff or random-phase approximations, commonly referred to as TDA and RPA respectively. We shall use

a similar approach for the above gas system. For simplicity, our calculation is done with a harmonic trap instead of the elongated traps as used in real experiments. Our calculation result indicates a sharp increase in frequency and damping rate in the transitional regime.

In the following, we shall first briefly describe the model space particle-hole Green's function method [78] which we shall employ. We shall use a small model space for the particle and hole orbits in solving the RPA/TDA equations, and hence the vertex functions have to be renormalized so that the contributions from orbitals outside the model space can be included. This renormalization leads to the reaction matrix interaction which we shall discuss in Section 4.3.

At low temperature and low particle density, the simple contact interaction $4\pi(\hbar/m)a_s\delta(r)$ is often used as an effective interaction for cold Fermi gas[80–83]. Such model interaction is suitable for weakly interacting system, where a_s is small. At crossover region when $a_s \to \infty$, this interaction becomes divergent. In such case the contact interaction must be first renormalized (or tamed) before input to microscopic calculation. We shall discuss that the well known Brueckner reaction matrix method, which has been widely and successfully used in nuclear matter [87–89] and finite nuclei [90], is very useful in this regard. We shall use this method to derive a renormalized atomic interaction which is smooth and well behaved at the Feshbach resonance. Our results together with some calculational details will be reported and discussed in the last section. A summary will also be presented.

4.2 Model space particle-hole Green's function method

In this section we briefly describe the model space particle-hole (ph) Green's function method [78] for calculating the quadrupole excitations of cold Fermi gas. We consider atoms as spin 1/2 fermions confined in a spherical harmonic oscillator potential of oscillator spacing $\hbar\omega_{osc}$ and oscillator length $a_{osc} = \sqrt{\hbar/m\omega_{osc}}$. We shall use $\hbar\omega_{osc}$ and a_{osc} respectively as the units for energy and length.

We treat the trapped gas as a closed shell system of N_F closed shells. For example, the $N_F = 6$ system has 112 atoms and in its unperturbed ground state the lowest 6 oscillator shells are completely filled. The excitation energies, denoted by E_n, of the system are calculated by solving the ph RPA equation [78, 79]

$$\begin{aligned} AX_n + BY_n &= E_n X_n, \\ -B^* X_n - A^* Y_n &= E_n Y_n. \end{aligned} \tag{4.1}$$

Here A represents the sum of the unperturbed ph energy gap and the TDA vertex function, namely

$$A(ph, p'h') = (\epsilon_p + S(p) - \epsilon_h - S(h))\delta_{ph,p'h'} + \Sigma(ph, p'h'), \tag{4.2}$$

where S denotes the one-body vertex function and Σ the two-body ph vertex function. They are composed of irreducible diagrams as illustrated in Fig. 4.1.

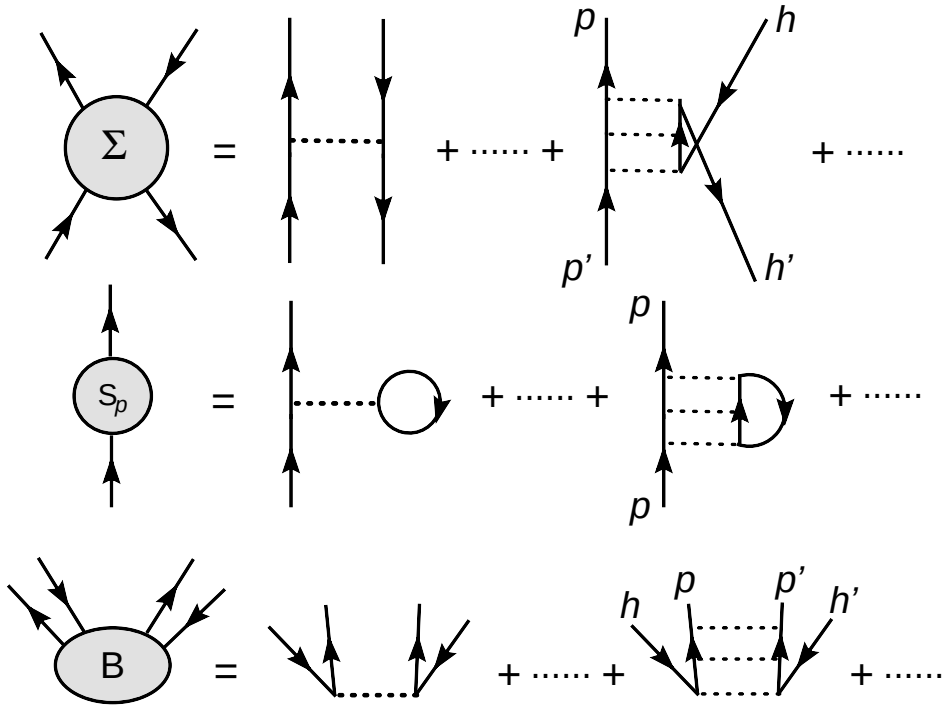

Figure 4.1: Diagrams for one- and two-body vertex functions. The dotted line vertex represents a V interaction.

Here each dashed-line represents the vertex of the effective atomic interaction V. Note that the diagrams are time ordered with retarded single particle propagators [78]. B denotes the ground-state correlation vertex, whose diagrammatic structure is also illustrated in Fig. 4.1. All the diagrams contained in the vertex function must be irreducible in the sense that any intermediate state of such diagrams must be orthogonal to the ph model space [78].

The transition amplitudes X and Y of Eqn. 4.1 are

$$X_n(ph) = \langle \Psi_n | a_p^\dagger a_h | \Psi_0 \rangle \tag{4.3}$$

$$Y_n(ph) = \langle \Psi_n | a_h^\dagger a_p | \Psi_0 \rangle, \tag{4.4}$$

where Ψ_n and Ψ_0 represent the nth excited- and ground-state wave functions respectively. When the ground state correlation vertex B is suppressed, Eqn. 4.1 becomes the TDA equation. We consider that the atomic gas is trapped by a harmonic oscillator potential. Thus ϵ of Eqn. 4.2 is the harmonic oscillator single particle energy.

In carrying out the RPA/TDA calculations, a restricted model space near the Fermi surface is employed. We use a hole space consisted of three major shells immediately below the Fermi surface, namely shells N_F to $(N_F - 2)$, and for particles one major shell immediately above. The external lines p, h, p' and h' of the vertex function diagrams of Fig. 4.1 are all confined in this space. That we use a restricted model space requires a model-space renormalization, so that the effects from the orbitals outside the model space are taken care of. The inclusion of the higher order diagrams in the vertex functions is for this renormalization purpose. As an example, let us consider the third order diagrams of Fig. 4.1. They all have a common "ladder" structure, with repeated interactions between a pair particle lines. The intermediate states of them include all the particle states outside the model space, so that our ph calculation within a small model space have renormalization contributions from the space outside. As discussed later, this type of "ladder" diagrams can be summed up to all orders, giving rise to the reaction matrix interaction.

4.3 Separable reaction matrix interaction

In carrying out our microscopic particle-hole calculations, we must first have an atomic interaction on which our many-body calculation is based. This

commonly used effective interaction for low temperature and low density cold quantum gas [80–83] is

$$V = 4\pi \frac{\hbar^2}{m} a_s \delta(r), \tag{4.5}$$

where m denotes the atomic mass, and a_s is the s-wave scattering length which can be tuned across the Feshbach resonance, essentially from $-\infty$ to $+\infty$. The above is an effective interaction for one hyperfine channel, in the sense that we consider atoms as of only one hyperfine state with the other hyperfine states having been integrated out by renormalization. In our calculation we assume atoms interacting with s-wave interactions only.

The above interaction is clearly divergent at the Feshbach resonance (the unitary limit) where $a_s \to \pm\infty$, and there is difficulty in using it in microscopic calculations. As described in Section 4.2, to carry out the TDA/RPA calculations, we need first calculate the vertex functions S, Σ and B. As illustrated in Fig. 4.1, these vertex functions are composed of irreducible diagrams. Near the Feshbach resonance, the above atomic interaction is divergent and consequently every diagram in the figure is divergent; calculation can not go on unless we use a different approach. This type of difficulty has been well known in nuclear matter theory and has been overcome by the Brueckner reaction matrix theory [87–89]. There each vertex of the bare nucleon-nucleon interaction V_{NN} is nearly divergent because of its very strong repulsive core. However, the Brueckner reaction matrix G given by the all order summation of the V_{NN} interactions between a pair of nucleons is finite and well behaved.

We apply a similar reaction matrix approach to our present atomic gas calculation. Let us consider the diagrams for the one-body vertex function S

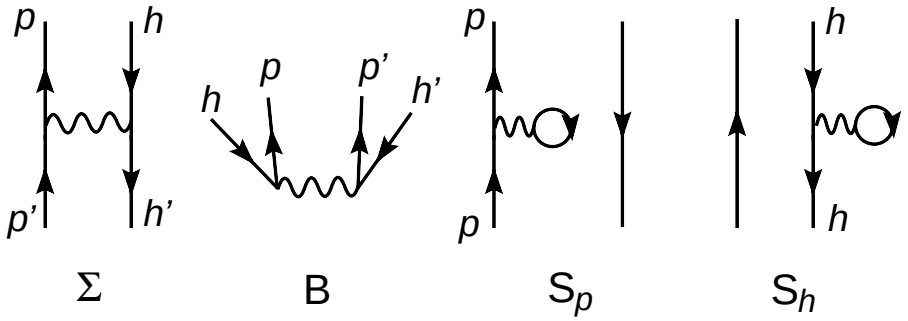

Figure 4.2: First-order R-matrix (wavy-line vertex) diagrams for one- and two-body vertex functions.

of Fig. 4.1. Clearly they have the structure of a geometric series and can be summed up to all orders. Let us define a reaction matrix R as

$$R = V + V\frac{Q}{e}V + V\frac{Q}{e}V\frac{Q}{e}V + ... = V + V\frac{Q}{e}R, \tag{4.6}$$

where e stands for $(\omega - H_0 + i0^+)$ and Q the Pauli exclusion operator. (Recall that we use time-ordered diagrams with retarded single particle propagators.) H_0 is the unperturbed Hamiltonian for the pair of interacting atoms, and ω is the starting energy which we shall discuss later. The role of Q is to ensure that the intermediate states of R must be outside of the chosen model space. In terms of R, the sum of all the ladder-type diagrams as shown by $S(p)$ of Fig.1 is now $\langle ph|R|ph\rangle$. Similarly the sum for Σ is $\langle ph'|R|p'h\rangle$ and for B is $\langle pp'|R|hh'\rangle$. We shall include only diagrams first order in R for the vertex function as listed in Fig. 4.2.

In calculating R, we shall use an angle average approximation [88] for the Pauli operator, namely Q is approximated by $Q_{av}(q, k_F)$ where q is the relative momentum and k_F is an average Fermi momentum which can be estimated

by using for example a local density approximation. In addition, we shall use plane-wave intermediate states and an average starting energy ω. Accurate methods for calculating the nuclear reaction matrix have been developed [90], and we plan to use them in a future work. With these approximations, the above R matrix becomes

$$R(k,k',\omega) = V(k,k') + \frac{2}{\pi}\int_0^\infty V(k,q)\frac{Q_{av}(q,k_F)}{\omega - q^2 + i0^+}R(q,k',\omega)q^2dq, \qquad (4.7)$$

where k, k', q are the relative momenta.

Let us now consider the above R matrix for the scattering length dependent potential of Eqn. 4.5. Schematically, R is given by $R = V/(1 - VQ/e)$ and may have well defined limits as $V \to \pm\infty$. But how to obtain them accurately is a difficult task in general, and it may not be feasible to obtain them reliably using numerical methods. We feel that R has to be solved analytically in order to obtain the above limits reliably. In this regard, we resort to the separable potential approach which has been widely used in nuclear physics [84–86]; the reaction matrix with this approach can be analytically solved. We shall use a separable potential which corresponds to a simulation of the potential of Eqn. 4.5 by a short range non-local Yukawa potential of the form $a_s e^{-\mu r}e^{-\mu r'}/(\mu^2 r r')$, μ^{-1} being the range of the interaction and r and r' the inter-atomic radial distance. We shall use large μ to simulate short range potential. In momentum space this potential becomes

$$V(k,k') = a_s\alpha f(k)f(k');\ f(q) = \frac{1}{\mu^2+q^2},\ \alpha = 8\pi\frac{\hbar^2}{m}\frac{\mu^3}{a_{osc}}. \qquad (4.8)$$

With this separable potential, the reaction matrix, which is complex, is also separable and is obtained analytically as

$$R(k,k',\omega) = [\eta_{re}(\mu,\omega) + i\eta_{im}(\mu,\omega)]f(k)f(k'), \tag{4.9}$$

with

$$\begin{aligned}
\eta_{re}(\mu,\omega) &= \frac{\lambda(\mu,\omega)}{D(\mu,\omega)}, \\
\eta_{im}(\mu,\omega) &= \frac{-\lambda(\mu,\omega)^2\sqrt{\omega}}{D(\mu,\omega)(\mu^2+\omega)^2}, \\
D(\mu,\omega) &= 1 + \frac{\omega\lambda(\mu,\omega)^2}{(\mu^2+\omega)^4}, \\
\lambda(\mu,\omega) &= \frac{a_s\alpha}{1-a_s\alpha I(\mu,\omega)}.
\end{aligned} \tag{4.10}$$

Note that $\eta_{im} = 0$ if $\omega < 0$. In the above, I is the integral

$$I(\mu,\omega) = \frac{2}{\pi}P\int_0^\infty \frac{Q_{av}(k,k_F)}{(\omega-k^2)(\mu^2+k^2)^2}k^2dk, \tag{4.11}$$

where P denotes principal value integration.

It is readily seen that R has well defined limits as $a_s \to \pm\infty$. Only the factor λ of Eqn. 4.10 is dependent on a_s, and at the above limits it becomes

$$\lambda_{\pm\infty}(\mu,\omega) = \frac{-1}{I(\mu,\omega)}. \tag{4.12}$$

Thus our R-matrix has a common well defined limit at the Feshbach resonance, being the same whether $a_s \to +\infty$ or $a_s \to -\infty$.

For dilute systems, k_F should be small. We have calculated the above R

matrix for several values of k_F, and found that the results for R calculated with k_F ranging from 0 to 1 are quite close to each other. For the case of $k_F = 0$ and $\omega > 0$, the integral of Eqn. 4.11 becomes

$$I(\mu, \omega) = \frac{\omega - \mu^2}{2\mu(\omega + \mu^2)^2}, \tag{4.13}$$

which is only weakly energy dependent if ω is much smaller than μ^2. Thus our R-matrix interaction is nearly energy independent for cold (small ω) dilute (small k_F) system with a short-range (large μ) interaction.

4.4 Results and discussion

We now describe some details about our calculations for the energy and decay width of the quadrupole excitation. They are obtained from the solutions of the RPA/TDA Eqn. 4.1, using the vertex functions given by the diagrams of Fig. 4.2. These diagrams are calculated from the R-matrix interaction, using the methods detailed in [90]. Since R is complex, Eqn. 4.1 is now a complex equation and its eigenvalues E_n are generally complex. We write E_n as $(ReE_n - i\Gamma_n)$, with the decay width given by Γ_n. In Fig. 4.3 we present results for the lowest 2^+ state of an N_F=8 (240 atoms) model system, using parameters k_F=0.3, ω=1 and μ=20. (We have also calculated N_F=6 and 7 systems, with results both being highly similar to those of $N_F = 8$.) These parameters should be suitable for cold dilute systems interacting with a short range interaction. The above choice has the advantage of making R-matrix weakly energy dependent as we have $\mu^2 >> \omega$. As shown, our calculated

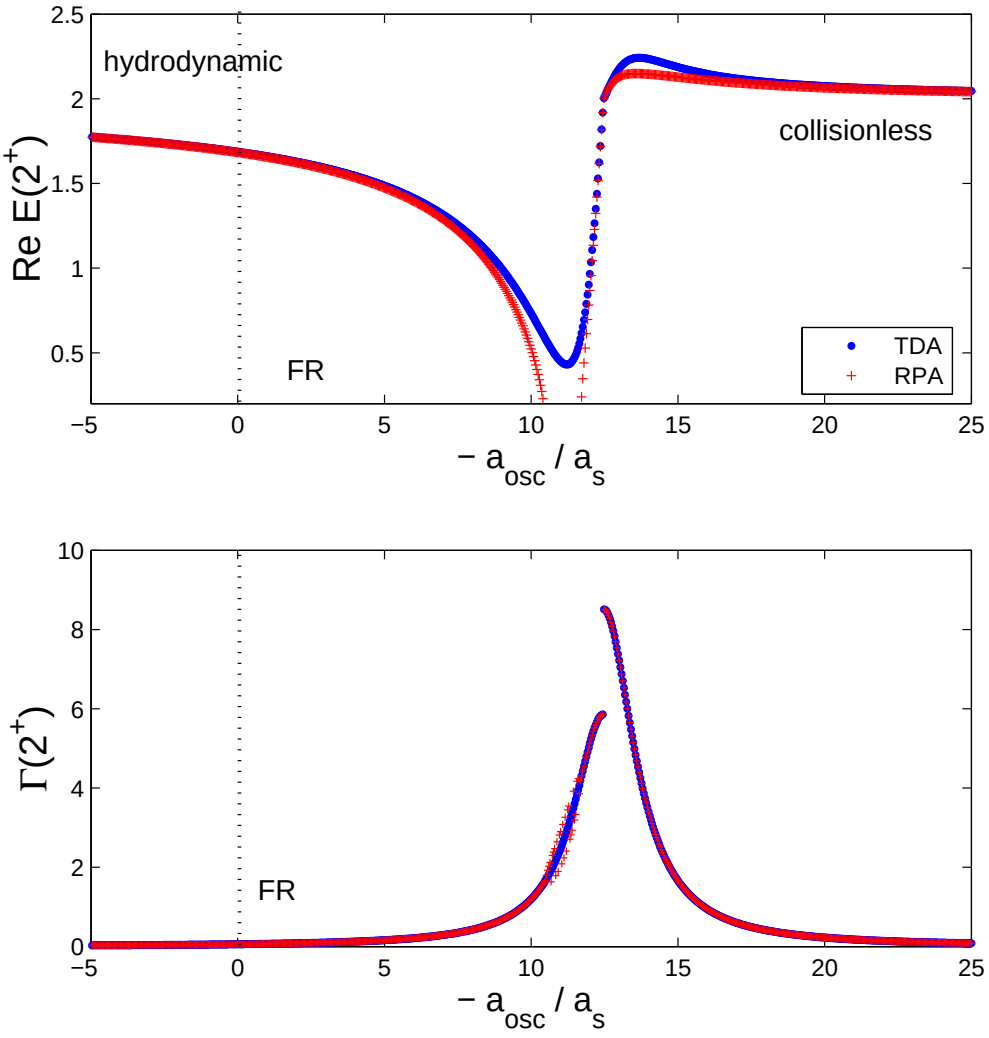

Figure 4.3: Energy and decay width of the quadrupole excitation.

energy at Feshbach resonance (FR) is about 1.7 $\hbar\omega_{osc}$ with nearly zero width, both being smooth functions there.

The shapes of our calculated spectrum and decay width are worth noting. Starting from the left end of Fig. 4.3, ReE exhibits a gradual drop followed by an abrupt rise and finally remains nearly constant. At both ends, ReE approaches to 2. Most importantly, the decay width Γ is peaked concurrently with the abrupt rise, both happening right at a_λ. These specific features of our results agree remarkably well with experiments on the radial compression model [22, 25] and the radial quadrupole model[27] in trapped cold ^{6}Li gas.

The above abrupt rising feature is mainly due to the R-matrix interaction. The factor λ of Eqn. 4.10 has a pole when a_s equals to $a_\lambda = -1/(\alpha I)$. It is readily seen that at a_λ the imaginary part of the R matrix is peaked with a Lorentzian form, while its real part vanishes. In addition, R is positive to the left of $(-a_{osc}/a_\lambda)$, and negative on the other side. These properties of R determine the general shapes of our results. For small k_F and ω, a_λ is close to $a_{osc}/4\pi$. In fact for k_F=0 and $\omega = 0$, a_λ is exactly equal to $a_{osc}/4\pi$, independent of μ. As shown in the figure, the abrupt rising takes place very close to 4π. We note that RPA and TDA give nearly identical results far from a_λ. Near a_λ, ReE for RPA tends to negative indicating the system being unstable.

Last but not least, Γ is discontinuous at a_λ as shown. We have found that the wave functions X and Y of Eqn. 4.1 are also discontinuous at a_λ. Such unusual features deserves further investigation.

4.5 Conclusion

In summary, we have carried out a particle-hole shell model calculation for the quadrupole excitations of a model cold Fermi gas trapped in a harmonic potential. An essential step is the use of a reaction matrix renormalized interaction. Using a separable potential approach, this interaction has been derived analytically and it is a smooth function at Feshbach resonance although the atomic interaction before renormalization is divergent there. Our results demonstrate that, in between the hydrodynamic and collisionless regimes, trapped cold Fermi gas undergoes a transition with abrupt variations in both energy (frequency) and decay width (damping rate), in qualitative agreement with experiments in cold alkali gas on the radial compression mode and the radial quadrupole mode.

Chapter 5

Brueckner reaction matrix and its application to cold Fermi gas at the unitary limit

5.1 Introduction

At the unitary limit, cold Fermi gas should exhibit universal behavior in a sense that physical properties of the gas are independent on the underlying two-body interaction. Such universality has been introduced in Chapter 1 of this dissertation.

In Chapter 3 we presented a study of neutron matter at and near the unitary limit[41]. Through a manual tuning on the mass of σ meson in the CD-Bonn potential[40], the bare neutron-neutron interaction is modified to result in a huge ${}^1S_0$ scattering length of -12000fm. The total energy per neutron E_0/A is then computed with an infinite-order summation of ring di-

agrams, and the expected 'universal' equation of state at zero temperature and at the unitary limit, namely, $E_0/A = \xi(3/10)k_F^2(\hbar = m = 1)$, is obtained with $\xi = 0.44$. Such work is based on a model space approach, where the bare neutron-neutron interaction properly renormalized with either the low-momentum potential V_{low-k} or the Brueckner G-matrix. The resulting value of ξ agrees well with results from recent quantum Monte Carlo computations [38, 39] and experiments on trapped cold alkali gas[32, 35–37].

Brueckner G-matrix has been widely used in nuclear physics. In this Chapter we shall present another study of cold fermi gas at the unitary limit where the G-matrix is applied. Owing to the hard core singularity and the tensor-force components, the bare nucleon-nucleon(NN) interaction is unsuitable for direct input to microscopic calculations. The G-matrix is constructed from the bare NN interaction through a ladder resummation. Taking into account the presence of the medium around individual nucleons, the intermediate states in the ladder summation are restricted to particles states only. In other words, apart from the binary scattering, the effect of the Pauli exclusion is also taken into consideration in the construction of G.

The use of G-matrix for an analytical derivation of ξ has been considered by other authors[92]. These derivations are complicated by the ambiguity in the starting energy ω. Usually one assume a certain value of ω and obtain an approximation or a numerical bound for ξ. In this Chapter we carried out a fully self-consistent zero-temperature Brueckner-Hartree-Fock(BHF)[91] computation on the total energy for a low-density Fermi gas. In other words, ω is determined self-consistently and is not a parameter taking on a certain

value by assumption. At the unitary limit we obtained

$$\frac{E_0^{BHF}}{A} = 0.54 \cdot \frac{3}{10} k_F^2, \tag{5.1}$$

higher than the result of $0.44(3/10)k_F^2$ from our ring-diagram computation. According to a recent study of cold Fermi gas with quantum Monte Carlo method[38], the total energy per particle of the *normal* ground state at the unitary limit is also $0.54(3/10)k_F^2$. Our result suggests that a fully *self-consistent* BHF approach at the unitary limit well captures the properties of the *normal* ground state. To be discussed later, the BHF theory also provide direct and important physical insights into how the strongly interacting particles at and around the unitary limit can be described and predicted from a simple Hartree-Fock picture with an effective interaction.

5.2 Method outline

Let us first outline the essential steps of the Brueckner-Hartree-Fock approach. The well-known BHF theory [91] has been specifically developed for treating strongly interacting many-body systems. A central quantity in this theory is the Brueckner reaction matrix, commonly referred to as the G-matrix. The BHF theory has been widely used for describing strongly interacting nuclear systems, including both finite nuclei and nuclear matter. Consider a many body system with Hamiltonian $H = H_0 + V$ where H_0 is the unperturbed Hamiltonian and V a two-body interaction. The ground state energies of H and H_0 shall be denoted as E_0 and W_0 respectively. In BHF theory, the

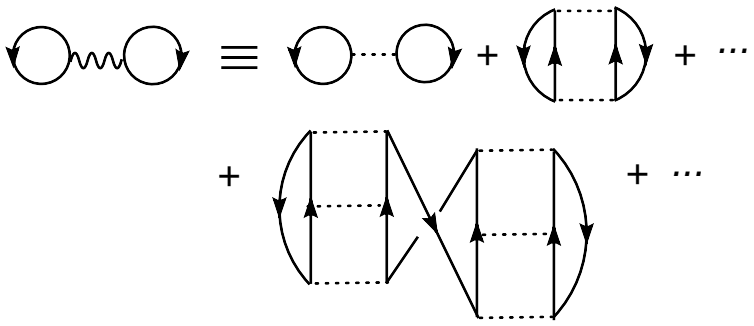

Figure 5.1: Diagrams summed in Brueckner-Hartree-Fock calculation on the ground state energy.

ground state energy shift $\Delta E_0 \equiv E_0 - W_0$ is given by the all-order sum of the two-hole-line linked diagrams as shown in Fig.5.1. Note that the intermediate particle lines of these diagrams are all above the Fermi momentum k_F. Note also that self-energy insertions are included only for the hole lines, as indicated by the third diagram of the figure. In this way, ΔE_0 is obtained by solving the following set of self-consistent equations:

$$\Delta E_0 = \sum_{a,b \le k_F} \langle a,b|G(\omega = \epsilon_a + \epsilon_b)|a,b\rangle, \tag{5.2}$$

$$\epsilon_a = \frac{k_a^2}{2} + \langle a|U|a\rangle, \tag{5.3}$$

$$\begin{aligned} \langle a|U|a\rangle &= \sum_{h \le k_F} \langle a,h|G(\omega = \epsilon_a + \epsilon_h)|a,h\rangle, \ a < k_F \\ &= 0, \ \textit{otherwise}. \end{aligned} \tag{5.4}$$

In the above U is the single-particle potential and ϵ the self-consistent single-particle energy.

The in-medium G-matrix is defined by

$$G(\omega) = V + V g_B(\omega) G(\omega);\ g_B(\omega) \equiv \frac{Q_{>F}}{\omega - H_0}, \tag{5.5}$$

where the Pauli exclusion operator $Q_{>F}$ is to ensure that the intermediate states of G are beyond the Fermi surface. In contrast, the reaction matrix R for the two-particle scattering in vacuum is given by

$$R(\omega) = V + V g(\omega) R(\omega);\ g(\omega) \equiv \frac{\mathcal{P}}{\omega - H_0}, \tag{5.6}$$

where g is the propagator in free space. $\mathcal{P}$ refers to Principal Value calculation. Through Eqn.(5.5) and (5.6), G-matrix can be expressed in terms of the scattering length a_s and k_F as will be shown in the next section.

5.3 Brueckner G-matrix in low-density systems

The universality of degenerate Fermi gas at the unitary limit have been discussed in earlier Chapters. The properties of any such system is determined by the Fermi momentum k_F in the same unique way, irrespective of the details of the underlying two-body potential. Both the low-density condition (small k_F) [16] and a small effective range (r_e) [60] have been stressed as the necessary criteria for universality.

The Brueckner G-matrix of a low-density Fermi gas, when expressed in terms of the scattering parameters (a_s and r_e) and k_F, indeed acquires a simple

and 'universal' form as long as $k_F \ll \mu$ where μ denotes the range of the two-body interaction in k-space. To illustrate this we shall employ an exactly solvable model. Suppose

$$\begin{aligned} V(k,k') &= V_0,\ k,k' \leq \mu \\ &= 0,\ otherwise. \end{aligned} \tag{5.7}$$

where k, k' are relative momenta. The momentum space integral equation for the reaction matrix R is

$$R(k,k',\omega_)) = V(k,k') + \frac{2}{\pi} P \int_0^\infty V(k,q) \frac{1}{\omega - q^2} R(q,k',\omega_0) q^2 dq. \tag{5.8}$$

The above equation can be readily solved for s-wave and the scattering length is determined by the potential strength V_0 and the potential range μ by

$$\frac{1}{a_s} = \frac{1}{V_0} + \frac{2\mu}{\pi}. \tag{5.9}$$

Similarly, the Brueckner G-matrix can first be solved in terms of V_0, and then expressed in terms of a_s through the above relation. For positive energies $\omega = k_0^2 > 0$, we have the exact solution

$$\begin{aligned} G(k,k',\omega) &= G_0,\ k,k' \leq \mu \\ &= 0,\ otherwise, \end{aligned} \tag{5.10}$$

with

$$G_0 = \frac{1}{\frac{1}{a_s} - \frac{2}{\pi}k_F - \frac{2}{\pi}\frac{k_0}{2}\ln\frac{(\mu+k_0)(k_F-k_0)}{(\mu-k_0)(k_F+k_0)}}. \tag{5.11}$$

Obviously, if $k_F \ll \mu$, the length scale μ drops out and leaves

$$G_0 = \frac{1}{\frac{1}{a_s} - \frac{2}{\pi}k_F + \frac{2}{\pi}k_0\tanh^{-1}(\frac{k_0}{k_F})}. \tag{5.12}$$

Within a self-consistent approach, ω is *not* a free parameter but has to be determined by a self-consistent procedure. Thus the Brueckner G-matrix above is only determined by a_s and k_F. At the unitary limit where $a_s^{-1} = 0$, k_F is the only length scale left.

More generally, for an arbitrary potential V, the G-matrix is related to the R-matrix through the relation

$$G(\omega) - R(\omega) = R(\omega)\left(g_B(\omega) - g(\omega)\right)G(\omega). \tag{5.13}$$

For a *sufficiently low* density $k_F \ll \mu$, the low-momentum components of G and R can be safely taken as constant while the high-momentum components are exactly canceled through $(g_B - g)$. We thus have an expression for the G-matrix for such low-density systems, denoted by $G_{low-\rho}$ as follows:

$$G_{low-\rho}(\omega) = \frac{1}{\frac{1}{R(\omega)} + \frac{2}{\pi}(-k_F + k_0\tanh^{-1}(k_0/k_F))} \tag{5.14}$$

$R(\omega)$ can be expanded through the effective range approximation

$$-\frac{1}{R(\omega)} = -\frac{1}{a_s} + \frac{1}{2}r_e\omega + \cdots \tag{5.15}$$

Under the assumption of a small effective range r_e, one can see that $G_{low-\rho}$ simply reduces to the expression G_0 as derived from a model interaction.

The derivation for negative energies $\omega < 0$ are similar. In summary, the form of the G-matrix for low-density systems with a negligible effective range is

$$\begin{aligned} & G_{low-\rho}(\omega) \\ = & \frac{1}{\frac{1}{a_s} - \frac{2}{\pi}k_F + \frac{2}{\pi}k_0 \tanh^{-1}(\frac{k_0}{k_F})} \quad \omega = k_0^2 > 0 \\ = & \frac{1}{\frac{1}{a_s} - \frac{2}{\pi}k_F + \frac{2}{\pi}\kappa_0 \tan^{-1}(\frac{\kappa_0}{k_F})} \quad \omega = -\kappa_0^2 < 0. \end{aligned} \tag{5.16}$$

(Through the relation $\tanh^{-1}(ix) = i\tan^{-1}(x)$, the two expressions reduce to one if the tanh function is taken as complex.)

Mathematically, the quantity $G_{low-\rho}(\omega)$ has a very simple structure. Physically, it is particularly useful to illustrate the interplay of different length scales like a_s, k_F and r_e in the effective interaction between individual particles in the vicinity of the unitary limit.

Alternatively, at the unitary limit, the dropping out of the length scale a_s and the universality can also be understood through the relation between the Brueckner G-matrix and the wave function of the quasi-bound state ψ_0. It can be easily shown that

$$G(a_s^{-1} \to 0) \simeq \frac{|\chi_0\rangle\langle\chi_0|}{\langle\chi_0|g - g_B|\chi_0\rangle}, \tag{5.17}$$

where $|\chi_0\rangle \equiv H_0|\psi_0\rangle$. The zero-energy wave function ψ_0 is 'everywhere flat' outside the range of the interaction, thus the low-momentum parts of χ_0 is

practically independent of the underlying potential.

In the next section, we shall apply $G_{low-\rho}$ in a fully self-consistent BHF computation to obtain the total energy of a cold Fermi gas. As we shall see below, the calculation with $G_{low-\rho}$ takes on a very simple form owing to the simplicity in $G_{low-\rho}$ itself.

5.4 Self-consistent BHF computation

We shall compute the total energy per particle E_0^{BHF}/A for a two-species degenerate Fermi gas at zero temperature using the Brueckener-Hatree-Fock method. The computation is based on $G_{low-\rho}(\omega)$ which is the Brueckner G-matrix derived under a low-density condition and the assumption of a negligible effective range.

Around the unitary limit $a_s^{-1} = 0$, one can expand E_0^{BHF} in powers of the small parameter $(a_s k_F)^{-1}$, giving

$$\frac{E_0^{BHF}}{E_0^{free}} = a_0 - \frac{a_1}{a_s k_F} - \frac{a_2}{(a_s k_F)^2} + O(\frac{1}{(a_s k_F)^3}) \tag{5.18}$$

where E_0^{free} is the total energy in a two-species non-interacting Fermi gas. The expansion coefficients a_0, a_1, and a_2 *et.al.* are universal in the sense of being independent of the underlying two-body potential.

In BHF theory, the potential energy can be obtained by summing up the matrix elements $\langle \mathbf{k_1}, \mathbf{k_2}| \, G(\omega) \, |\mathbf{k_1}, \mathbf{k_2}\rangle$ for all $\mathbf{k_1}, \mathbf{k_2}$ inside the Fermi sphere, with ω to be determined through a self-consistent procedure. As mentioned, for low-density systems with a small effective range, one simply need the low-

momentum components of G. Therefore, one can use $G_{low-\rho}$ in place. Also, around the unitary limit where a_s is huge, we can consider the contribution from s-wave only. Expressed in terms of the relative ($\mathbf{k}$) and center-of-mass ($\mathbf{K}$) momenta, the potential energy per particle is simply

$$\frac{PE^{BHF}}{A} = \frac{3}{8\pi k_F^3}\frac{2}{\pi}\int_0^{k_F}\int_{\mathcal{R}} G_{low-\rho}(\omega)k^2 \mathrm{d}\mathbf{K}\mathrm{d}k \tag{5.19}$$

, where $k = |\mathbf{k}|$, and $\mathcal{R}$ is the appropriate integration region for the center-of-mass $\mathbf{K}$. $G_{low-\rho}(\omega)$ is in the basis of the spherical Bessel functions and this explains the $2/\pi$ factor. The integration with respect to $\mathbf{K}$ introduces the factor

$$... \int_{\mathcal{R}} \mathrm{d}\mathbf{K} ... = ...8 \cdot \frac{4\pi k_F^3}{3}\left(1 - \frac{3k}{2k_F} + \frac{k^3}{2k_F^3}\right)... \tag{5.20}$$

The potential energy is then be readily obtained with any trial value of ω.

As from Eqn.(5.16), the energy-dependence of $G_{low-\rho}(\omega)$ comes from the tanh function in the denominator. This makes $G_{low-\rho}(\omega)$ a slowly varying function in the neighborhood of $\omega = 0$. Fig.5.2 shows a plot of $G_{low-\rho}(\omega)$ particularly at the unitary limit $a_s^{-1} = 0$. It may seem reasonable to simplify the calculation by taking the so-called 'low-energy' limit $\omega = 0$. However, as to be discussed later, the self-consistency procedure is indeed very crucial and the final result will differ significantly from simply setting $\omega = 0$ throughout.

To incorporate a self-consistent BHF computation, we follow standard pro-

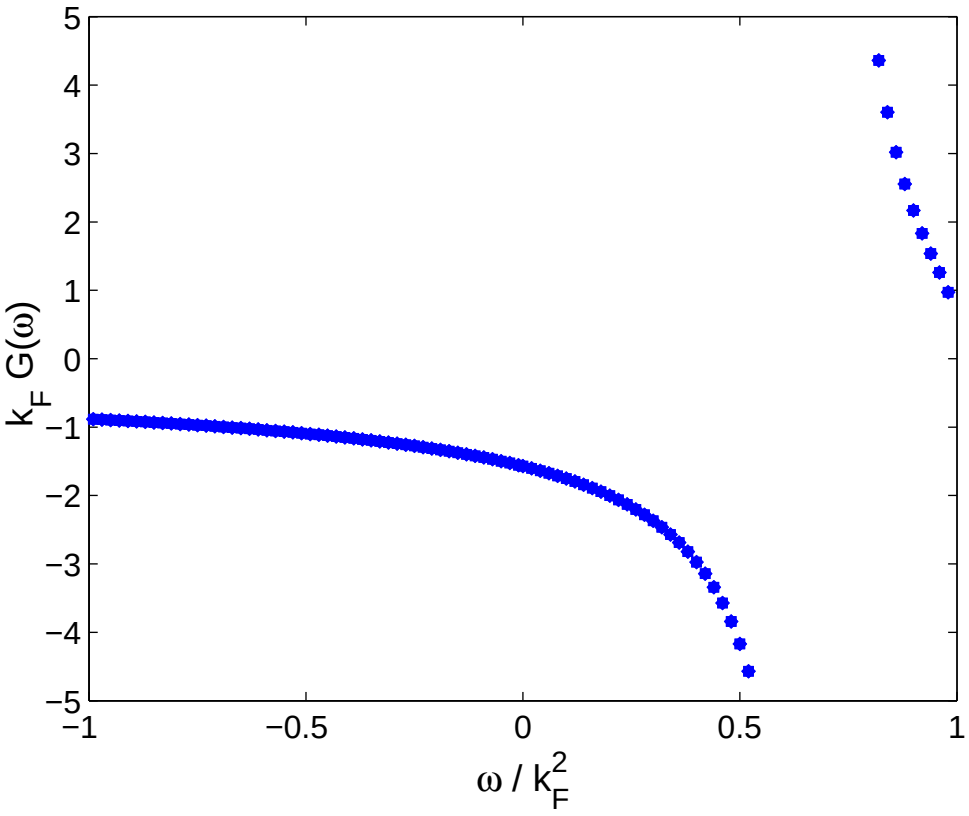

Figure 5.2: $G_{low-\rho}(\omega)$ in unit of k_F^{-1}. The energy ω is normalized by k_F^2.

cedures used in nuclear physics. The single-particle energies are given by

$$\begin{aligned}
\epsilon(k) &= \frac{k^2}{2} + \frac{16}{\pi}\int_0^{\frac{k_F-k}{2}} k'^2 G(\omega)\mathrm{d}k' \\
&+\frac{8}{\pi}\int_{\frac{k_F-k}{2}}^{\frac{k_F+k}{2}} k'^2\left(1-\frac{k'^2+k^2/4-k_F^2/4}{kk'}\right)G(\omega)\mathrm{d}k' \\
&\qquad\qquad\qquad\qquad\qquad\qquad\qquad\qquad k<k_F \\
&= \frac{8}{\pi}\int_{\frac{k-k_F}{2}}^{\frac{k+k_F}{2}} k'^2\left(1-\frac{k'^2+k^2/4-k_F^2/4}{kk'}\right)G(\omega)\mathrm{d}k' \\
&\qquad\qquad\qquad\qquad\qquad\qquad\qquad\qquad k\geq k_F. \qquad (5.21)
\end{aligned}$$

where the factors comes from the angular integrations. The effective mass m^* is defined by a quadratic fit on $\epsilon(k)$, namely

$$\epsilon(k) = \frac{k^2}{2m^*} + \Delta. \tag{5.22}$$

The self-consistency requires

$$\omega = \frac{k^2}{m^*} + 2\Delta + \frac{K^2}{4}(\frac{1}{m^*} - 1). \tag{5.23}$$

The last term above comes from the center-of-mass energy, and is treated with a standard center-of-mass averaging that gives

$$\frac{K_{av}^2}{4} = \frac{\frac{3}{5}k_F^2\left(1 - \frac{k}{k_F}\right)\left(1 + \frac{k}{2k_F} + \frac{k^2}{6k_F^2}\right)}{1 + \frac{k}{2k_F}}. \tag{5.24}$$

Eqn.(5.21),(5.23) and (5.19) are iterated until convergence is reached. Our primary interest is the region around unitarity, therefore a small neighborhood around $a_s^{-1} = 0$ is used, with various choices of k_F. Notice that in this work, both a_s^{-1} and k_F are in an arbitrary length unit. In our computations, the convergence rate is fast. Fig.5.3, 5.4 and 5.5 shows the results for $k_F = \{1.0, 2.0, 5.0, 8.0, 10.0\}$ over the range $a_s^{-1} \in [-0.2, 0.2]$. The universality at the point $a_s^{-1} = 0$ is particularly clear from the plot Fig.5.3 and 5.4.

At the unitary limit, namely $a_s^{-1} = 0$, we get $m^* = 1.13$, $\Delta = -0.81\varepsilon_F$ and $E_0^{BHF} = 0.54E_0^{free}$, where where $\varepsilon_F = \frac{3}{5}\frac{k_F^2}{2}$ is the energy per particle in a two-species free Fermi gas. From a quantum Monte Carlo study[38], the ground state energy of a two-species Fermi gas at the unitary limit is also

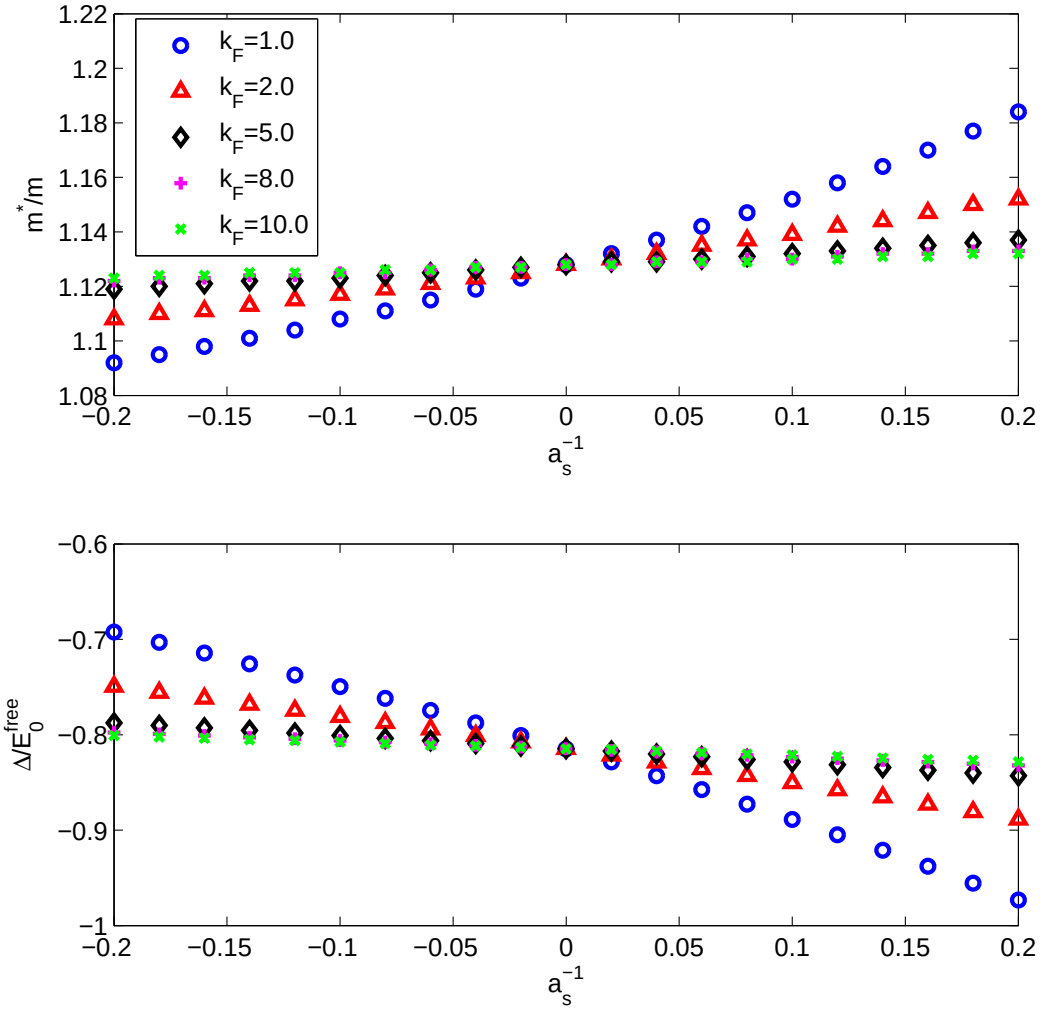

Figure 5.3: Self-consistent BHF computation results for the ground state properties of a two-species fermion system over the range $(a_s k_F)^{-1} \in \{-0.02, 0.02\}$. Note that both a_s and k_F are in an arbitrary length unit.

$0.54E_0^{free}$ with trial wave-functions being Slater determinants. This excellent agreement shows that the self-consistent BHF theory with $G_{low-\rho}$ well captures the properties of the *normal* ground state of all cold Fermi gas at the unitary limit.

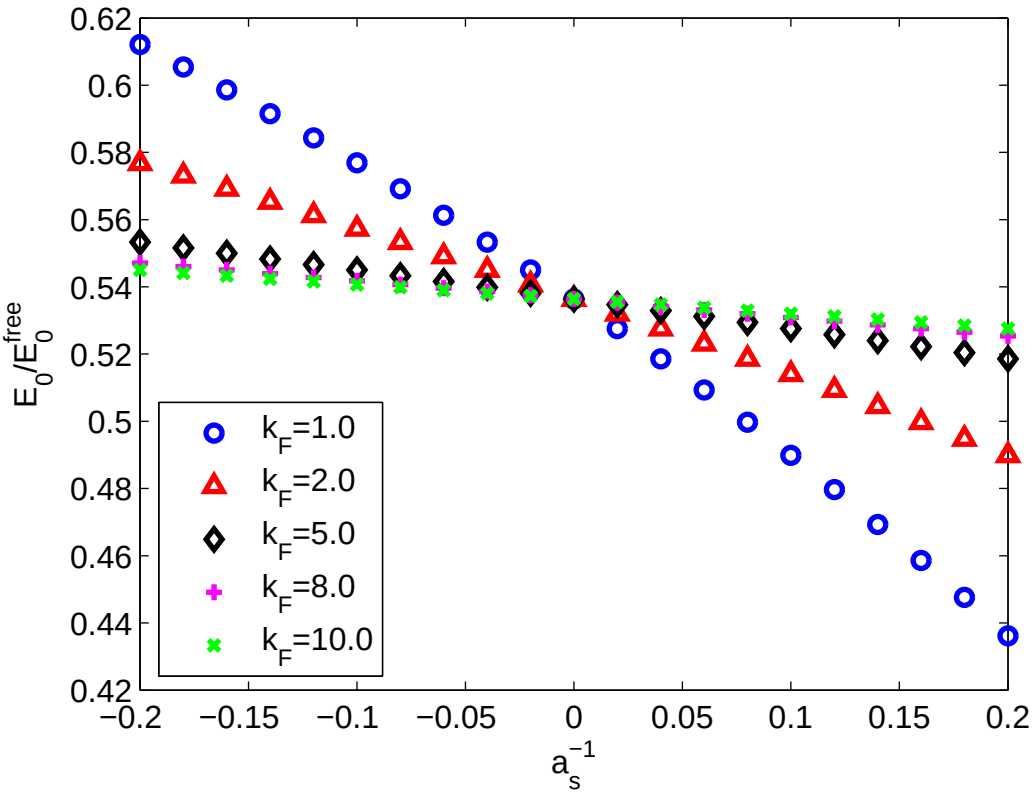

Figure 5.4: Self-consistent BHF computation results for the ground state energy of a two-species fermion system over the range $(a_s k_F)^{-1} \in \{-0.02, 0.02\}$.Note that both a_s and k_F are in an arbitrary length unit.

To obtain the higher-order expansion coefficients a_1 and a_s in Eqn.5.18,a least-square fitting is done on the 105 data points in Fig.5.4 with a fitting curve $E_0^{BHF}/E_0^{free} = a_0 - \frac{a_1}{a_s k_F} - \frac{a_2}{(a_s k_F)^2}$. We got $a_0 = 0.54$, $a_1 = 0.44$ and $a_2 = 0.31$. The fitting curve and the data points are plotted together in Fig.5.5.

The single-particle spectrum $\epsilon(k)$ at the unitary limit is of much interest. Within the BHF formalism, the spectrum is self-consistently determined. In Fig.5.6 we plot the fully converged spectrum for the case $k_F = 1.0$ and $a_s^{-1} = 0$. Notice that the spectrum $\epsilon(k)$ is well described by the quadratic relation

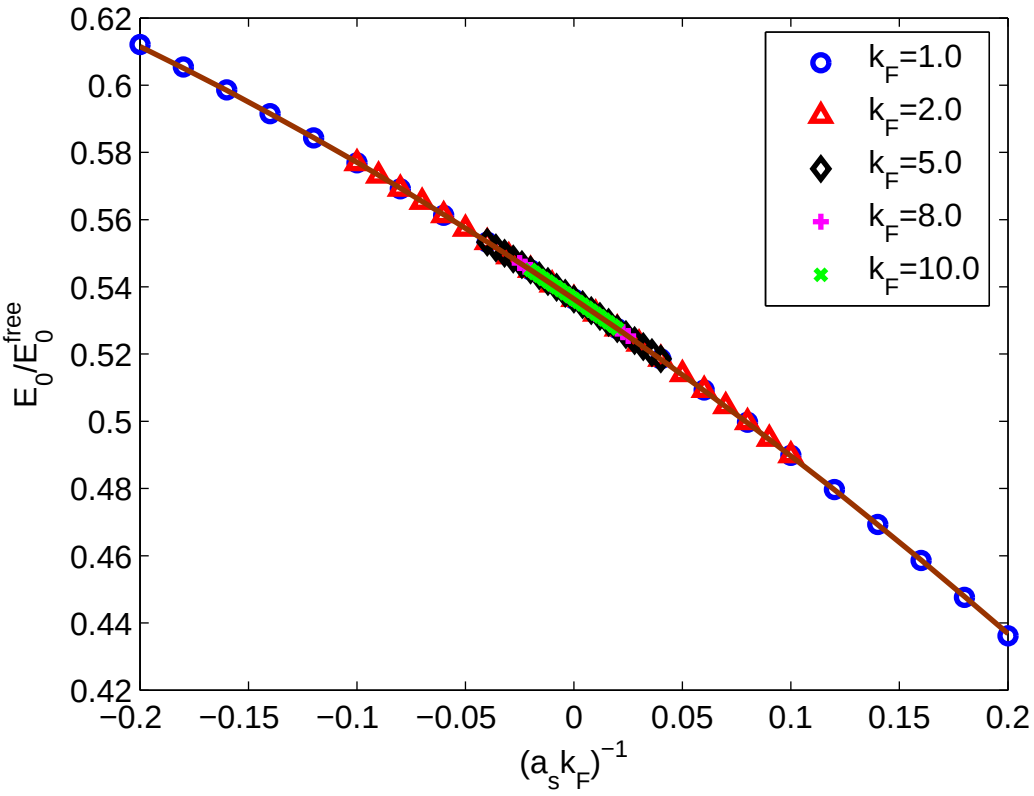

Figure 5.5: The data in Fig.5.4 is plotted here with a fitting curve $E_0^{BHF}/E_0^{free} = a_0 - \frac{a_1}{a_s k_F} - \frac{a_2}{(a_s k_F)^2}$.

$\epsilon(k) = \frac{k^2}{2m^*} + \Delta$ as in Eqn.5.22.

As mentioned, at the unitary limit we obtained an effective mass $m^* = 1.13(\hbar = m = 1)$ slightly larger than the bare mass m. However, in the unit of the energy per particle in a free gas $\varepsilon_F = \frac{3}{5}\frac{k_F^2}{2}$, we got $\Delta = -0.81\varepsilon_F$ which is comparable to ε_F. In Fig.5.6 we normalize the single-particle energy ϵ with the energy scale k_F^2.

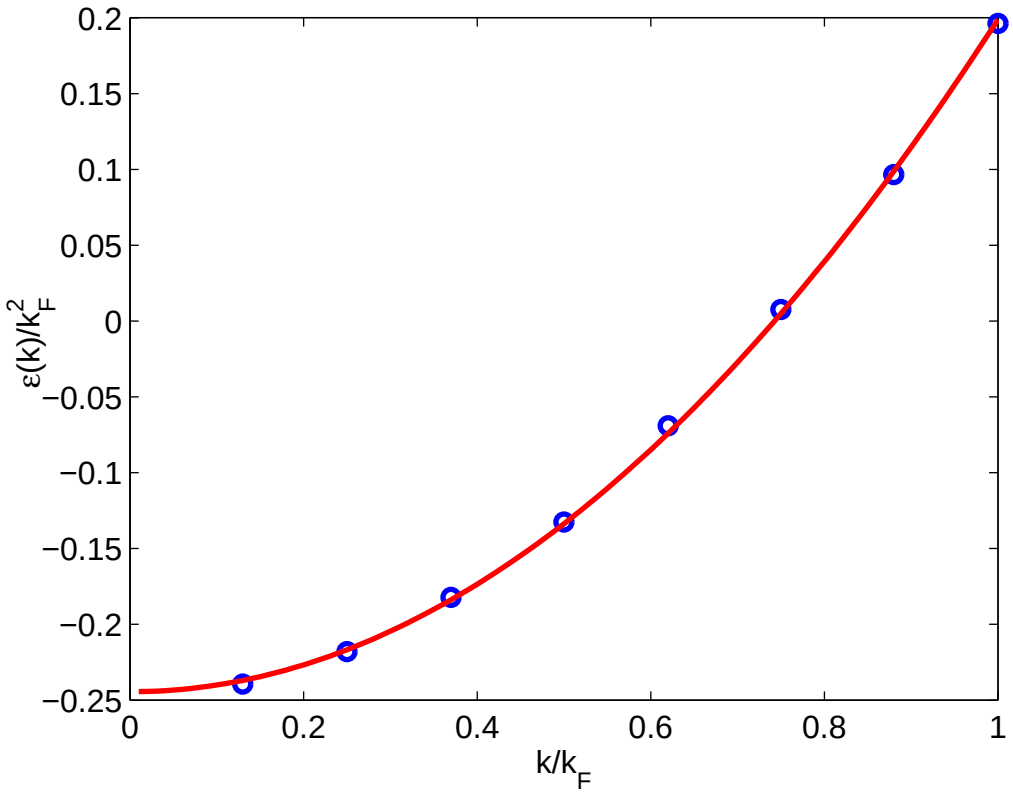

Figure 5.6: Fully converged data of the single-spectrum $\epsilon(k)$ for the case $k_F = 1.0$ and $a_s^{-1} = 0$, with a fitting curve of the form $\epsilon(k) = \frac{k^2}{2m^*} + \Delta$. Notice that $\epsilon(k)$ is normalized by k_F^2.

5.5 Brueckner G-matrix at the unitary limit as a schematic effective interaction

As pointed out in Chapter 3, the equation of state of cold Fermi gas at or close to the unitary limit can be reproduced by a schematic effective interaction of the form

$$V_{FS} = \frac{1}{\frac{S}{a_s} - \frac{2}{\pi}k_F} \tag{5.25}$$

($\hbar = m = 1$) where S is a positive parameter satisfying $S \ll |a_s|$. By direct observation such effective interaction looks highly similar to the expression $G_{low-\rho}(\omega = 0)$. Recall that

$$G_{low-\rho}(\omega = 0) = \frac{1}{\frac{1}{a_s} - \frac{2}{\pi}k_F}. \tag{5.26}$$

Obviously it is only determined by two length scales, namely a_s and k_F. The appearance of k_F in expression comes from the Pauli operator. Within the BHF formalism or the model space ring-diagram computation presented before, ω is not a free parameter and must be consistently determined. Nonetheless, by direction observation $G_{low-\rho}(\omega = 0)$ as an effective interaction at the unitary limit can indeed reproduce the expected equation of state with a simple Hartree-Fock picture. More quantitatively, assuming that only s-wave contributes (true at the unitary limit), the potential energy of a cold Fermi gas with a contact interaction given by $G_{low-\rho}(\omega = 0)$ can be computed easily:

$$\frac{PE}{A} = \frac{2}{\pi}\frac{k_F^3}{6}\frac{1}{\frac{1}{a_s} - \frac{2}{\pi}k_F} \tag{5.27}$$

which is also equivalent to

$$\frac{PE}{KE} = \frac{10k_F}{9\pi}\frac{1}{\frac{1}{a_s} - \frac{2}{\pi}k_F}. \tag{5.28}$$

It follows then the total ground state energy is

$$\frac{E}{E^0_{free}} = \frac{4}{9} - \frac{5\pi}{18}\frac{1}{a_s k_F} - \frac{5\pi^2}{36}\frac{1}{(a_s k_F)^2} + O(\frac{1}{(a_s k_F)^3}. \tag{5.29}$$

At the unitary limit where $1/a_s = 0$, the total energy extracted equals $4E_0^{free}/9$, surprisingly close to the value of $0.44E_0^{free}$ from our ring-diagram summation method. It would be of much interest if one can show via rigorous derivations that an all-order particle-particle hole-hole ring-diagram summation at the unitary limit can be 'reduced' to a simple first-order Hartree-Fock sum with an effective interaction of $G_{low-\rho}(\omega = 0)$.

5.6 Conclusion

In this Chapter, we studied the ground state properties of a two-species cold Fermi gas with a fully self-consistent Brueckner-Hartree-Fock(BHF) approach. Under the assumption of a low density and a small effective range, the total energy per particle E_0^{BHF}/A is found to be an universal expression of $0.54(3k_F^2/10)$ at the unitary limit. The single-particle spectrum is determined to be $\epsilon(k) = k^2/(2m^*) + \Delta$ where $m^* = 1.13$ and $\Delta = -0.81(3k_F^2/10)(m = \hbar = 1)$. Our result is in excellent agreement with the result from quantum Monte Carlo method on the normal ground state at the unitary limit[38], which also gives $0.54(3k_F^2/10)$.

Chapter 6

Summary

In this dissertation we studied cold Fermi systems at and close to the unitary limit. Such strong interacting systems can be experimentally explored with trapped cold alkali atoms. Making use of magnetic field induced Feshbach resonances, experimentalists managed to tune the interactions between two different spin states, turning trapped cold atoms into unique many-body systems with tunable interactions. Close to a Feshbach resonance, the scattering length a_s of cold atoms can be tuned through a wide range, essentially from $-\infty$ to ∞. Low-density cold Fermi gas with an infinite scattering length is of particular interest, often described as at the 'unitary limit', these systems are predicted to have universal properties. More specifically, their properties should be determined only by the density or the Fermi momentum k_F, and become independent of the underlying two-body interactions.

At the unitary limit, the universal equation of state at zero-temperature of cold Fermi gas can be shown to be $E_0 = \xi E_0^{free}$ where E_0^{free} is the energy of a free Fermi gas. We have calculated the universal constant ξ with neutron

matter. Starting from the meson-exchange CD-Bonn potential, we constructed neutron-neutron potentials with various $^1S_0$ scattering lengths such as $a_s = -12070$fm and $+21$fm. At the limit of $a_s \to \pm\infty$, our calculated ratio of E_0 to that of the non-interacting case is found remarkably close to a constant over a wide range of Fermi momenta. Our results confirms the expected universality in cold Fermi gas and the extracted value $\xi = 0.44$ is also in excellent agreement with results from quantum Monte Carlo studies, which were taken as the most accurate estimate on ξ by far.

In the calculation of E_0 we have carried out a model space ring-diagram summation, in which the low-momentum particle-particle hole-hole ring diagrams are summed up to all orders. In such calculation renormalized neutron-neutron interactions are employed. We have stressed on the advantage of using the recently developed low-momentum potential V_{low-k} over the traditionally used Brueckner G-matrix in our model space calculation.

We have also studied the collective excitations of cold Fermi gas. The recent measurements on the certain excitation modes reveal a region close to a Feshbach resonance where a cold Fermi system transits from the hydrodynamic regime to the collisionless regime. An abrupt rise in oscillation frequency with a large decay rate was observed signifying such transition. With a model cold Fermi system trapped in a harmonic potential, we performed a particle-hole Green's function calculation on a quadrupole excitation. Both the Tamm-Dancoff and random phase approximations revealed a rise in frequency accompanied with a large decay width.

Bibliography

[1] C.J. Pethick and H. Smith, Bose-Einstein Condenstion in Dilute Gases, Cambride, 2002.

[2] A. Einstein, Sitzungsberichte der Preussischen Akademie der Wissenschaften, Physikalisch-mathematische Klasse 261 (1924); 3 (1925).

[3] M. H. Anderson, J. R. Ensher, M. R. Matthews, C. E. Wieman, and E. A. Cornell, Science **269**, 198 (1995).

[4] A.J. Leggett, J. Phys. C **41**, 7 (1980).

[5] P. Noziers and S. Schmitt-Rink, J. Low Temp. Phys. **59**, 195 (1985).

[6] E.Tiesinga, B.J.Verhaar and H.T.C. Stoof, Phys. Rev. A, **47** 4114 (1993).

[7] S. Inouye, M.R. Andrews, J. Stenger, H.J. Miesner, D.M. Stamper-Kurn and W. Ketterle, Nature, **392** 151 (1998).

[8] T. Loftus, C.A. Regal, C. Ticknor, J.L. Bohn and D.S. Jin, Phys. Rev. Lett., **88** 173201 (2002).

[9] C. Chin, M. Bartenstein, A. Altmeyer, S. Riedl, S. Jochim, J. Hecker Denschlag, R. Grimm, Science **305**, 1128 (2004).

[10] M. Greiner, C.A. Regal and D.S. Jin, Phys. Rev. Lett. **94**, 070403 (2005).

[11] C.A. Regal, M. Greiner and D.S. Jin, Phys. Rev. Lett. **92**, 040403 (2004).

[12] M.W. Zwierlein, C.A. Stan, C.H. Schunck, S.M.F. Raupach, A.J. Kerman and W. Ketterle, **92**, 120403 (2004).

[13] M.W. Zwierlein, J.R. Abo-Shaeer, A. Schirotzek, C.H. Schunck and W. Ketterle Nature, **435**, 1047 (2005).

[14] M. Bartenstein, A. Altmeyer, S. Riedl, R. Geursen, S. Jochim, C. Chin, J. Hecker Denschlag, R. Grimm, A. Simoni, E. Tiesinga, C. J. Williams, P. S. Julienne, Phys. Rev. Lett. **94** 103201 (2005).

[15] G. A. Baker, Jr., Phys. Rev. C **60**, 054311 (1999).

[16] H. Heiselberg, Phys. Rev. A **63**, 043606 (2001).

[17] T.L. Ho, Phys. Rev. Lett. **92**, 090402 (2004).

[18] S. Stringari, Europhys. Lett. **65**, 749 (2004).

[19] A. Bulgac and G. F. Bertsch, Phys. Rev. Lett. **94**, 070401 (2005).

[20] H. Heiselberg, Phys. Rev. Lett. **93**, 040402 (2004).

[21] J. Kinast, S.L. Hemmer, M.E. Gehm, A. Turlapov, and J.E. Thomas, Phys. Rev. Lett. **92**, 150402 (2004).

[22] J. Kinast, A. Turlapov, and J. E. Thomas, Phys. Rev. A **70**, 051401(R) (2004).

[32] J. Kinast, A. Turlapov, and J. E. Thomas, Phys. Rev. Lett. **94**, 170404 (2005).

[24] A. Turlapov, J. Kinast,B. Clancy, Le Luo, J. Joseph, J.E. Thomas, J Low Temp. Phys. **150**, 567 (2008).

[25] M. Bartenstein, A. Altmeyer, S. Riedl, S. Jochim, C. Chin, J. Hecker Denschlag, and R. Grimm Phys. Rev. Lett. **92**, 203201 (2004).

[26] A. Altmeyer, S. Riedl, C. Kohstall, M. J. Wright, R. Geursen, M. Bartenstein, C. Chin, J. Hecker Denschlag, and R. Grimm, Phys. Rev. Lett. **98**, 040401 (2007).

[27] A. Altmeyer, S. Riedl, M.J. Wright, C. Kohstall, J. Hecker Denschlag, R. Grimm, Phys. Rev. A **76**, 033610 (2007).

[28] M.J. Wright, S. Riedl, A. Altmeyer, C. Kohstall, E.R. Sánchez Guajardo, J. Hecker Denschlag, and R. Grimm, Phys. Rev. Lett. **99**, 150403 (2007).

[29] A. Bulgac, Phys. Rev. Lett. **95**, 140403 (2005).

[30] A. Bulgac, Joaquín E. Drut, and Piotr Magierski, Phys. Rev. Lett. **96**, 090404 (2006).

[31] A. Bulgac, Joaquín E. Drut, and Piotr Magierski, Phys. Rev. Lett. **99**, 120401 (2007).

[32] J. Kinast, A. Turlapov, J.E. Thomas, Q. Chen, J. Staijc and K. Levin, Science **307**, 1296

[33] J. E. Thomas, J. Kinast, and A. Turlapov, Phys. Rev. Lett. **95**, 120402 (2005).

[34] R. F. Bishop, Int. J. Mod. Phys. B 15, iii (2001), Many-Body Challenge Problem by G. F. Bertsch.

[35] T. Bourdel, L. Khaykovich, J. Cubizolles, J. Zhang, F. Chevy, M. Teichmann, L. Tarruell, S. J. J. M. F. Kokkelmans, and C. Salomon, Phys. Rev. Lett. **93**, 050401 (2004).

[36] G. B. Partridge, W. Li, R. I. Kamar, Y.-A. Liao, and R. G. Hulet, Science **311**, 503 (2006).

[37] J. T. Stewart, J. P. Gaebler, C. A. Regal, and D. S. Jin, Phys. Rev. Lett **97** 220406 (2006).

[38] J. Carlson, S.-Y. Chang, V. R. Pandharipande, and K. E. Schmidt, Phys. Rev. Lett. **91**, 050401 (2003).

[39] G. E. Astrakharchik, J. Boronat, J. Casulleras, and S. Giorgini, Phys. Rev. Lett. **93**, 200404 (2004).

[40] R. Machleidt, Phys. Rev. C **63**, 024001 (2001).

[41] L.-W. Siu, T. T. S. Kuo and R. Machledit, Phys. Rev. C **77**, 034001 (2008).

[42] G.E. Brown, M. Rho, Phys. Rev. Lett. **66**, 2720 (1991).

[43] G.E. Brown, M. Rho, Phys. Rept. **396**, 1 (2004).

[44] L.-W. Siu, J.W. Holt, T.T.S. Kuo and G.E. Brown, in preparation.

[45] K. A. Brueckner, C. A. Levinson, and H. M. Mahmoud, Phys. Rev. **95**, 217 (1954);

[46] H. A. Bethe, Annu. Rev. Nucl. Sci. **21**, 93 (1971).

[47] R. B. Wiringa, V.G.J. Stoks and R. Schiavilla, Phys. Rev. C **51**, 38 (1995).

[48] V.G.J. Stoks, R.A.M. Klomp, C.P.F. Terheggen and J.J. de Swart, Phys. Rev. C **49**, 2950 (1994).

[49] D.R. Entem, R. Machleidt, Phys. Rev. C **68**, 041001 (2003).

[50] S.K. Bogner, T.T.S. Kuo and L. Coraggio, Nucl. Phys. **A684**, 432 (2001).

[51] S.K. Bogner, T.T.S. Kuo, L. Coraggio, A. Covello and N. Itaco, Phys. Rev. C **65**, 051301R (2002).

[52] L. Coraggio, A. Covello, A. Gargano, N. Itako, T.T.S. Kuo, D.R. Entem and R. Machleidt, Phys. Rev. C **66**, 021303(R) (2002).

[53] A. Schwenk, G.E. Brown and B. Friman, Nucl. Phys. **A703**, 745 (2002).

[54] S.K. Bogner, T.T.S. Kuo and A. Schwenk, Phys. Rep. **386**, 1 (2003).

[55] J.D. Holt, T.T.S. Kuo and G.E. Brown, Phys. Rev. C **69**, 034329 (2004).

[56] S.K. Bogner, A. Schwenk, T.T.S. Kuo and G.E. Brown, arXiv:nucl-th/0111042.

[57] H. Feshbach, Ann. Phys. **19**, 287 (1962).

[58] T. Köhler, K. Góral and P.S. Julienne, Rev. Mod. Phys. **78**, 1311 (2006).

[59] C.H. Schunck, M.W. Zwierlein, C.A. Stan, S.M.F. Raupach, W. Ketterle, A. Simoni, E. Tiesinga, C.J. Williams and P.S. Julienne, Phys. Rev. A **71**, 045601 (2005).

[60] G.M. Bruun, Phys. Rev. A **70**, 053602 (2004).

[61] S. Simonucci, P. Pieri and G.C. Strinati, Europhys. Lett. **69**, 713 (2005).

[62] A. Perali, P. Pieri, and G. C. Strinati, Phys. Rev. Lett. **93**, 100404 (2004).

[63] Y. Nishida, and D. T. Son, Phys. Rev. Lett. **97**, 050403 (2006).

[64] R. Haussmann, W. Rantner, S. Cerrito, and W. Zwerger, Phys. Rev. A **75**, 023610 (2007).

[65] J.-W. Chen, and E. Nakano, Phys. Rev. A **75**, 043620 (2007).

[66] A. Schwenk and C. J. Pethick, Phys. Rev. Lett. **95**, 160401 (2005).

[67] D. Lee and T. Schäfer, Phys. Rev. C **73**, 015202 (2006).

[68] H.Q. Song, S.D. Yang and T.T.S. Kuo, Nucl. Phys. **A462**, 491 (1987).

[69] H. A. Bethe, Annu. Rev. Nucl. Sci. **21**, 93 (1971).

[70] J.W. Holt and G.E. Brown, p.239 in Hans Bethe and His Physics (World Scientific, July 2006, editted by G.E. Brown and C.-H. Lee).

[71] K. Suzuki and S. Y. Lee, Prog. Theor. Phys. **64**, 2091 (1980).

[72] F. Andreozzi, Phys. Rev. C **54**, 684 (1996).

[73] R. Rapp, R. Machleidt, J.W. Durso and G.E. Brown, Phys. Rev. Lett. **82**, 1827 (1999).

[74] R. Grimm in Ultracold Fermi Gases, Procs. of the Int. School of Physics "Enrico Fermi", Course CLXIV, Varenna, 20 - 30 June 2006 edt. by M. Inguscio, W. Ketterle, and C. Salomon.

[75] S. Giorgini, L.P. Pitaevskii, S. Stringari, arXiv:0706.3360.

[76] D.T. Son, Phys. Rev. Lett. **98**, 020604 (2007).

[77] J. Speth and J. Wambach, Int. Rev. Nucl. Phys. **7**,1 (1991) (World Scientific).

[78] S.S. Wu and T.T.S. Kuo, Nucl. Phys. **A430**, 110 (1984).

[79] J. Blomqvist, T.T.S. Kuo and G.E. Brown, Phys. Lett. **31B**, 93 (1970).

[80] H.T.C. Stoof, M. Bijlsma, and M. Houbiers, J. Res. Natl. Inst. Stand. Tech. **101**, 443 (1996).

[81] A.J. Leggett, Rev. Mod. Phys. **73, No.2**, (2001).

[82] H. Heiselberg and B. Mottelson, Phys. Rev. Lett. **88**, 190401 (2002).

[83] P.F. Bedaque and U. van Kolck, Annu. Rev. Nucl. Part. Sci. **52**, 339 (2002).

[84] G.E. Brown and M. Bolsterli, Phys. Rev. Lett. **3**, 472 (1959).

[85] F. Tabakin, Ann. Phys. (NY) **30**, 51 (1964).

[86] D.J. Ernst C., M. Shakin, and R. M. Thaler, Phys. Rev. C **8**, 46 (1973).

[87] J.P. Jeukenne, A. Lejeune, C. Mahaux, Phys. Rep. **25**, 83 (1976).

[88] T.T.S. Kuo, Z. Y. Ma, and R. Vinh Mau, Phys. Rev. C **33**, 717 (1986).

[89] J.E. Holt and G.E. Brown, "Hans Bethe and His Physics" (World Scientific), 201 (2006).

[90] M. Hjorth-Jensen, T.T.S. Kuo ans E. Osnes, Phys. Rep. **261**, 125 (1995).

[91] K. A. Brueckner, C. A. Levinson, and H. M. Mahmoud, Phys. Rev. **95**, 217 (1954); H. A. Bethe, Phys. Rev. **103**, 1353 (1956); H. A. Bethe, Phys. Rev. **103**, 1353 (1956).

[92] T. Schäfer, C.-W. Kao, S.R. Cotanch, Nucl. Phys. **A762**, 82 (2005).